Ruthenium−Aminoallenylidene Complexes from Butatrienylidene Intermediates via an Aza-Cope Rearrangement: Synthetic, Spectroscopic, Electrochemical, Spectroelectrochemical, and Computational Studies

Rainer F. Winter* and Karl-Wilhelm Klinkhammer

Institut für Anorganische Chemie der Universität Stuttgart, Pfaffenwaldring 55, D-70569 Stuttgart, Germany

Stanislav Záliš*

J. Heyrovský Institute of Physical Chemistry, Academy of Sciences of the Czech Republic, Dolejškova 3, Prague, Czech Republic

Received October 31, 2000

Ruthenium−aminoallenylidene complexes *trans*-$[Cl(L_2)_2RuCCC(NR_2)CH_2R']^+EF_6^-$ (**4a**−**f**; E = P, Sb, L_2 = chelating diphosphine) are accessible from the respective dichloro precursors, $NaEF_6$, butadiyne, and an allylic amine in a one-pot procedure. The reactions proceed via the primary butatrienylidene intermediate *trans*-$[Cl(L_2)_2Ru{=}C{=}C{=}C{=}CH_2]^+$ and the initial addition products *trans*-$[Cl(L_2)_2Ru{-}C{\equiv}CC(NR_2R'){=}CH_2]^+$ via an Aza-Cope type rearrangement. Amine adducts have been isolated for (dimethylamino)-2-pentyne (**3f**) and 1-methyl-1,2,5,6-tetrahydropyridine (**3g**). The former cleanly converts to its aminoallenylidene isomer upon warming. All products have been characterized by various spectroscopic techniques, including NMR, IR, and UV/vis spectroscopy and cyclic voltammetry; complex **4b** was also characterized by X-ray crystallography. Most notable are the considerable bond length alternations along the unsaturated C_3 ligand and the trigonal-planar nitrogen, indicative of its sp^2 character. Aminoallenylidene complexes of this type are best described as a hybrid between true cumulenic and iminium alkynyl resonance forms, with major contributions of the latter, as is also evident from the high energy barriers for rotation around the iminium type C=N bond. The effect of the electron density on the metal on the spectroscopic and electrochemical properties of the cations in **4** has been probed for the dimethylallylamine-derived complexes *trans*-$[Cl(L_2)_2RuCCC(NMe_2)C_4H_7]^+EF_6^-$ (**4a**−**c**), which only differ in the nature of the chelating diphosphine ligand. Aminoallenylidene complexes **4** undergo reversible one-electron oxidation. In contrast, their reduction is irreversible at room temperature but partially reversible at temperatures between 233 and 195 K. The spectroscopic changes accompanying oxidation were monitored by in situ UV/vis, IR, and EPR techniques. DFT calculations have been performed on the model complexes *trans*-$[Cl(L_2)_2Ru{=}C{=}C{=}C{=}CH_2]^+$ and *trans*-$[Cl(L_2)_2RuC_3\{N(CH_3)_2\}CH_3]^+$. Our results explain the regioselectivity of nucleophilic addition to the proposed butatrienylidene intermediate and the spectroscopic and electrochemical properties of aminoallenylidene complexes **4**. Both orbital and steric effects are equally important in the regioselective addition to C_3. The calculations further indicate primarily metal-based oxidation and ligand-based reduction of complexes **4**, in accordance with experimental observations. They also let us assign the experimental UV/vis bands and the two main IR absorptions in the 2000−1500 cm^{-1} region.

Introduction

Within the context of transition-metal complexes containing higher homologues of the carbene ligand, the chemistry of butatrienylidene complexes has emerged as a fascinating research field on its own right. In principle, a cumulated C_4 ligand can function in several bonding modes, either as a bridging ligand in dimetal complexes or higher nuclearity transition-metal clusters or in mononuclear complexes in either the side-on (η^2) or end-on (η^1) binding mode. Cumulenic "naked" C_4 bridges as part of a more extended 1,6-dimetallahexapentaenylidene are present in the dianionic molybdenum and tungsten complexes $[\{Tp'(CO)_2M\}_2(\mu,\eta^1{:}\eta^1\text{-}C_4)]^{2-}$ (Tp′ = hydridotris(3,5-dimethylpyrazolyl)borate,

* To whom correspondence should be addressed. R.F.W.: e-mail, winter@iac.uni-stuttgart.de; fax, +49 711 685 4065. S.Z.: e-mail, stanislav.zalis@jh-inst.cas.cz; fax, +4202 858 2307.

10.1021/om000925n CCC: $20.00
Publication on Web 03/08/2001

M = Mo, W)[1] or in various oxidized forms of butadiynediyl-bridged dirhenium,[2a−c] dimanganese,[2d] diiron,[3] or diruthenium[4] complexes. Cumulenic butatrienylidene entities have also been invoked as significant contributors in a trioxidized, diynediyl-derived diiron complex[5] and the zwitterionic resonance form of a C_4-bridged rhenium−triosmium cluster.[6] The diiron complexes [{Cp*L_2Fe}=C=C=C=C(R){Fe(CO)$_2$Cp*}] (L = ^{i}Pr$_2$-PC_2H_4P^{i}Pr$_2$, dppe; R = H, Me), where butatrienylidene ligands span two different iron centers, were reported to arise from the protonation or methylation of the respective diynediyl-bridged precursor.[7] Butatrienylidene ligands C_4RH (R = $SiMe_3$, H) have also been found in pentanuclear ruthenium clusters, where they employ two C=C π bonds for additional side-on coordination and thus act as six-electron donors.[8]

Two more general approaches to stable mononuclear complexes with an end-on butatrienylidene ligand are now available. The first consists of the activation of terminal alkynyl keto complexes {M}−C≡CC(O)CHRR′ (or enol ethers thereof) with a formally OH-abstracting agent such as trifluoroacetic acid anhydride.[9,10] This method, as originally introduced by Selegue,[10] has ultimately rendered Cl(P^{i}Pr$_3$)$_2$Ir=C=C=C=CPh$_2$ as the first stable butatrienylidene complex that also lends itself to structural characterization by X-ray methods.[9] This compound owes its stability to protection of the terminal sp^2 carbon by aryl substituents, which is also the key to stable pentatetraenylidene complexes.[11] A more direct access route consists of the activation of terminal diynes by coordinatively unsaturated yet electron-rich transition-metal fragments.[12−15] This methodology is akin to the well-known alkyne to vinylidene tautomerization.[16] Although this approach has not produced any stable butatrienylidene species to date, the outcome of diverse trapping reactions convincingly supports their presence as reactive intermediates.

With regard to the reactivity of the terminal butatrienylidene ligand, the primary system derived from butadiyne has received the most attention and seems to differ substantially from that of its mono- and disubstituted secondary or tertiary analogues. Its reactivity patterns have initially been rationalized by the alternating of electrophilic (C_1, C_3) and nucleophilic (C_2) carbon centers along the cumulenic chain, as was suggested by semiempirical calculations.[17] DFT calculations on the *neutral electron-poor* d^6 complexes (CO)$_5$-Cr=C$_n$=CH$_2$ (n = 1−8), however, showed that polarization of the carbon chain is almost negligible and the observed regioselectivity is explained by frontier orbital control.[18] Thus, the C_4H_2 ligand regioselectively adds aprotic nucleophiles such as amines and phosphines to C_3, C_1 being sterically protected by the bulky coligands (usually tertiary phosphines) on the metal.[12a,c,13a,d] The protic nucleophiles ER_nH regioselectively add to the terminal C=C double bond to give substituted allenylidene complexes [{M}=C=C=C(ER_n)CH$_3$]$^{n+}$ (ER_n = NR_2,[12a,b] OR,[12a,b,15] SR,[13d] 2-(*N*-methylpyrrole[12a,b]), in which the nucleophilic center is again attached to C_3. In contrast, a secondary butatrienylidene complex derived from phenylbutadiyne is deprotonated by NEt_3 to give the phenylbutadiynyl complex,[14] while the tertiary butatrienylidene complex Cl(P^{i}Pr$_3$)$_2$Ir=C=C=C=CPh$_2$ adds trifluoroacetic acid to the *internal* C_2−C_3 double bond.[9]

The high synthetic potential of the primary butatrienylidene intermediates is highlighted by their cycloaddition/cycloreversion sequences with aromatic imines, yielding 4-ethynylquinolidine or vinyl-substituted 1-azabuta-1,3-diene complexes, depending on the substituents on the imine.[12c,d] We have already communicated an instance where the transient butenynyl complexes [Cl-(L_2)$_2$Ru−C≡CC(NMe$_2$allyl)=CH$_2$]$^+$, derived from amine addition to the respective butatrienylidene precursors (L_2 = Ph$_2$PCH$_2$Ph$_2$ (dppm), Et$_2$PC_2H_4PEt$_2$ (depe)), rearrange under very mild conditions via an Aza-Cope type process to the aminoallenylidene isomers [Cl(L_2)$_2$Ru=C=C=C(NMe$_2$)C_4H_7]$^+$. As such, this presents a rare example of a sigmatropic rearrangement occurring within the coordination sphere of a transition-metal

(1) Woodworth, B. E.; White, P. S.; Templeton, J. L. *J. Am. Chem. Soc.* **1997**, *119*, 828.
(2) (a) Seyler, J. W.; Weng, W.; Zhou, Y.; Gladysz, J. A. *Organometallics* **1993**, *12*, 3802. (b) Zhou, Y.; Seyler, J. W.; Weng, W.; Arif, A. M.; Gladysz, J. A. *J. Am. Chem. Soc.* **1993**, *115*, 8509. (c) Brady, M.; Weng, W.; Zhou, Y.; Seyler, J. W.; Amoroso, A. J.; Arif, A. M.; Böhme, M.; Frenking, G.; Gladysz, J. A. *J. Am. Chem. Soc.* **1997**, *119*, 775. (d) Kheradmandan, S.; Heinze, K.; Schmalle, H. W.; Berke, H. *Angew. Chem.* **1999**, *111*, 2412; *Angew. Chem., Int. Ed.* **1999**, *38*, 2270.
(3) Coat, F.; Guillemot, M.; Paul, F.; Lapinte, C. *J. Organomet. Chem.* **1999**, *578*, 76.
(4) (a) Bruce, M. I.; Denisovich, L. I.; Peregudova, S. M.; Ustynyuk, N. A. *Mendeleev Commun.* **1996**, 200. (b) Bruce, M. I.; Low, P. J.; Costuas, K.; Halet, J.-F.; Best, S. P.; Heath, G. A. *J. Am. Chem. Soc.* **2000**, *122*, 1949.
(5) Guillemot, M.; Toupet, L.; Lapinte, C. *Organometallics* **1998**, *17*, 1928.
(6) Falloon, S. B.; Arif, A. M.; Gladysz, J. A. *Chem. Commun.* **1997**, 629.
(7) Coat, F.; Guillemot, M.; Paul, F.; Lapinte, C. *J. Organomet. Chem.* **1999**, *578*, 76.
(8) (a) Adams, C. J.; Bruce, M. I.; Skelton, B. W.; White, A. H. *J. Chem. Soc., Chem. Commun.* **1996**, 2663. (b) Adams, C. J.; Bruce, M. I.; Skelton, B. W.; White, A. H. *J. Organomet. Chem.* **1999**, *584*, 254.
(9) Ilg, K.; Werner, H. *Angew. Chem.* **2000**, *112*, 1991; *Angew. Chem., Int. Ed.* **2000**, *39*, 1632.
(10) Lomprey, J. R.; Selegue, J. P. *Organometallics* **1993**, *12*, 616.
(11) (a) Romero, A.; Peron, D.; Dixneuf, P. H. *J. Chem. Soc., Chem. Commun.* **1990**, 1410. (b) Touchard, D.; Haquette, P.; Daridor, A.; Toupet, L.; Dixneuf, P. H. *J. Am. Chem. Soc.* **1994**, *116*, 11157. (c) Lass, R. W.; Steinert, P.; Wolf, J.; Werner, H. *Chem. Eur. J.* **1996**, *2*, 19. (b) Kovacik, I.; Laubender, M.; Werner, H. *Organometallics* **1997**, *16*, 5607.
(12) (a) Bruce, M. I.; Hinterding, P.; Low, P. J.; Skelton, B. W.; White, A. H. *J. Chem. Soc., Chem. Commun.* **1996**, 1009. (b) Bruce, M. I.; Hinterding, P.; Low, P. J.; Skelton, B. W.; White, A. H. *J. Chem. Soc., Dalton Trans.* **1998**, 467. (c) Bruce, M. I.; Hinterding, P.; Ke, M.; Low, P. J.; Skelton, B. W.; White, A. H. *J. Chem. Soc., Chem. Commun.* **1997**, 715. (d) Bruce, M. I.; Ke, M.; Kelly, B. D.; Low, P. J.; Smith, M. E.; Skelton, B. W.; White, A. H. *J. Organomet. Chem.* **1999**, *590*, 184−201.
(13) (a) Winter, R. F.; Hornung, F. M. *Organometallics* **1997**, *16*, 4248. (b) Winter, R. F. *J. Chem. Soc., Chem. Commun.* **1998**, 2209. (c) Winter, R. F. *Eur. J. Inorg. Chem.* **1999**, 2121. (d) Winter, R. F.; Hornung, F. M. *Organometallics* **1999**, *18*, 4005.
(14) Haquette, P.; Touchard, D.; Toupet, D.; Dixneuf, P. *J. Organomet. Chem.* **1998**, *565*, 67.
(15) Guillaume, V.; Thominot, P.; Coat, F.; Mari, A.; Lapinte, C. *J. Organomet. Chem.* **1998**, *565*, 75.
(16) (a) Lomprey, J. R.; Selegue, J. P. *J. Am. Chem. Soc.* **1992**, *114*, 5518. (b) Bullock, R. M. *J. Chem. Soc., Chem. Commun.* **1989**, 165. (c) Haquette, P.; Pirio, N.; Toupet, L.; Dixneuf, P. H. *J. Chem. Soc., Chem. Commun.* **1993**, 163. (d) Touchard, D.; Haquette, P.; Pirio, N.; Toupet, L.; Dixneuf, P. H. *Organometallics* **1993**, *12*, 3132. (e) Werner, H.; Rappert, T.; Wiedemann, R.; Wolf, J.; Mahr, N. *Organometallics* **1994**, *13*, 2721 (f) Whittall, I. R.; Humphrey, M. G.; Hockless, D. C. R.; Skelton, B. W.; White, A. H. *Organometallics* **1995**, *14*, 3970. (g) de los Ríos, I.; Jiménez-Tenorio, M.; Puerta, M. C.; Valerga, P. *J. Am. Chem. Soc.* **1997**, *119*, 6529. (h) Werner, H.; Lass, R. W.; Gevert, O.; Wolf, J. *Organometallics* **1997**, *16*, 4077.
(17) (a) Kostić, N. M.; Fenske, R. F. *Organometallics* **1992**, *1*, 974. (b) Schilling, B. E. R.; Hoffmann, R.; Lichtenberger, D. L. *J. Am. Chem. Soc.* **1979**, *101*, 585.
(18) Re, N.; Sgamellotti, A.; Floriani, C. *Organometallics* **2000**, *19*, 1115.

fragment.[19] Herein we present a full account of this work, including (i) an extension of this reaction to propargylic and functionalized allylic amines, (ii) the rearrangement of an *isolable* primary adduct to its aminoallenylidene isomer, (iii) full spectroscopic and electrochemical characterization of the products, (iv) the UV/vis, IR, and EPR spectroscopic characterization of some of the oxidized forms derived from the monocationic aminoallenylidene complexes, and (v) the results of DFT calculations on the $[Cl(PH_3)_4Ru{=}C{=}C{=}C{=}CH_2]^+$ and $[Cl(PH_3)_4RuCCC(NMe)_2CH_3]^{+/2+}$ model complexes, which complement previous calculations on butatrienylidene[17,18] and related allenylidene[20] compounds and aid in rationalizing the observed reactivity and spectroscopic properties of these systems in their closed- and open-shell forms.

Results and Discussion

Synthesis. We[13a,d] and others[12a,b] have previously reported on the trapping of ruthenium−butatrienylidene intermediates $[\{Ru\}{=}C{=}C{=}C{=}CH_2]^+$ ($\{Ru\}$ = $CpRu(PPh_3)_2$[12a,b]) and *trans*-$[Cl(dppm)_2Ru]$ (dppm = $Ph_2CH_2PPh_2$[13a,d]) generated in situ from the respective chloro precursors and excess butadiyne with tertiary amines. The stable 2-ammoniobutenynyl complexes $[Cl(dppm)_2Ru{-}C{\equiv}CC(NR_2R'){=}CH_2]^+$ (**3**) are obtained from a broad variety of aliphatic or benzylic amines or electron-rich pyridines by regioselective addition to carbon atom C_3 of the cumulated C_4 chain. If R′ is an allylic moiety, the primary addition products constitute quaternary vinyl allylammonium salts. Their purely organic counterparts may readily undergo 3-Aza-Cope (or 3-Amino-Claisen) rearrangements to their 1-azonia-1,5-hexadiene isomers. Although in many cases this process requires substantial thermal activation, such rearrangements have occasionally been observed under ambient or subambient conditions.[21] We have recently communicated that the dimethylallylamine-derived adducts $[Cl(L_2)_2Ru{-}C{\equiv}CC(NMe_2C_3H_5){=}CH_2]^+$ (L_2 = $Ph_2PCH_2Ph_2$ (dppm), $Et_2PC_2H_4PEt_2$ (depe)) also behave in this manner, providing rare examples of a sigmatropic rearrangement within the coordination sphere of a transition-metal complex.[19] The overall reaction sequence, i.e., addition of an aprotic, allyl-substituted nucleophile to butatrienylidene intermediates **2** followed by Cope- or Claisen-type rearrangements also constitutes one possible route to novel thio-[13c] or seleno-substituted[22] allenylidene complexes. We have now extended this protocol to a broader variety of allylic amines and a propargylic amine to explore its scope and limitations.

cis-$RuCl_2(dppm)_2$, excess butadiyne, and an appropriate allylic amine produce the respective amino-substituted allenylidene complexes **4a**,**d**,**e** in good to excellent yields in a one-pot synthesis with the concomitant formation of a ruthenium−carbon, a carbon−nitrogen, and a carbon−carbon bond and the cleavage of the nitrogen−allyl carbon bond (see Scheme 1). Simple allylic amines were successfully employed, but tris(2-methyl)allylamine failed to give any isolable product, most likely due to its steric bulk. Likewise, attempts to employ 1-benzyl-3-pyrroline as the trapping reagent gave a mixture of products from which the known *cis*-$[(dppm)_2RuCl(CH_3CN)]^+$ slowly crystallized. Since this complex is formed in the absence of any other nitrogen source, we feel that the nitrile ligand arises from the degradation of the amine. To probe for the effect of the electron density on the metal on the spectroscopic and electrochemical properties of complexes **4**, dimethylallylamine-derived analogues of **4a** with L_2 = dppe (**4b**), depe (**4c**) were also prepared, whereas the respective 1,2-bis(dicyclohexylphosphino)ethane derivative could not be obtained in this manner.

The primary adducts *trans*-$[Cl(dppm)_2Ru{-}C{\equiv}CC(NR_2R'){=}CH_2]^+$ were frequently identified at some early stage of these reactions by virtue of their characteristic IR band at 2032−2038 cm^{-1},[13a,d] but not isolated. This proved, however, possible for (dimethylamino)pent-2-yne as an example of a propargylic amine and 1-methyl-1,2,5,6-tetrahydropyridine, where the allylic moiety is confined to a heterocyclic ring. The respective 2-ammoniobutenynyl complexes **3f**,**g** were obtained in moderate yields after chromatographic workup. At somewhat elevated temperatures **3f** (above 60 °C) and **3g** (above 85 °C) react smoothly to the rearranged counterpart **4f** and an as yet unidentified product arising from **3g**. No clean rearrangement occurred for the ammoniobutenynyl complexes *trans*-$[Cl(dppm)_2Ru{-}C{\equiv}CC(NMe_2CH_2C_6H_4R){=}CH_2]^+$ (R = H, 3-OMe),[13d] where the aromatic double bond constitutes the allylic component. This contrasts to the numerous examples for thermally induced Amino-Claisen rearrangements of allyl-substituted anilines in organic chemistry, where the aromatic system serves as the vinylic part.[23] ^{31}P NMR spectra recorded during the gradual rearrangement of **3f** to **4f** at 80 °C are shown in Figure 1. Preliminary investigations show this process to obey simple first-order kinetics, as expected for an intramolecular reaction.

Our synthesis of the dppe complex **4b** deserves some special comment. Best results were achieved when the pure *trans* isomer was reacted with $NaSbF_6$ (or $NaPF_6$) in *o*-$C_6H_4Cl_2$ at room temperature. This is quite remarkable in that the *trans* isomer is usually regarded as being inert toward chloride dissociation under these conditions.[24] The more reactive *cis* isomer gave **4b** in moderate yield, while the use of $AgPF_6$, $AgCF_3SO_3$, and $TlPF_6$ as halide abstracting agents gave only intractable mixtures. Pure *trans*-$RuCl_2(dppe)_2$ is conveniently obtained in high yield, as detailed in the Experimental Section, whereas the *cis* isomer is always contaminated with the *trans* form.[25]

(19) Barrett, A. G. M.; Carpenter, N. E. *Organometallics* **1987**, *6*, 2249.

(20) (a) Cadierno, V.; Gamasa, M. P.; Gimeno, J.; González-Cueva, M.; Lastra, E.; Borge, J.; García-Granda, S.; Pérez-Carreño, E. *Organometallics* **1996**, *15*, 2137. (b) Esteruelas, M. A.; Gómez, A. V.; López, A. M.; Modrego, J.; Oñate, E. *Organometallics* **1997**, *16*, 5826. (c) Baya, M.; Crochet, P.; Esteruelas, M. A.; Gutiérrez-Puebla, E.; López, A. M.; Modrego, J.; Oñate, E.; Vela, N. *Organometallics* **2000**, *19*, 2585. (d) Berke, H.; Huttner, G.; von Seyerl, J. *Z. Naturforsch., B* **1981**, *36B*, 1277.

(21) (a) Vedejs, E.; Gingras, M. *J. Am. Chem. Soc.* **1994**, *116*, 579. (b) Walters, M. A.; Hoem, A. B.; McDonough, C. S. *J. Org. Chem.* **1996**, 55. (c) Walters, M. A. *J. Org. Chem.* **1996**, 978.

(22) Hartmann, S.; Winter, R. F.; Scheiring, T.; Wanner, M. *J. Organomet. Chem.*, in press.

(23) (a) Bennett, G. B. *Synthesis* **1977**, 589. (b) Heimgartner, H.; Hansen, H.-J.; Schmid, H. *Adv. Org. Chem.* **1979**, *9*, 655. (c) Lutz, R. P. *Chem. Rev.* **1984**, *84*, 205.

(24) Chin, B.; Lough, A. J.; Morris, R. H.; Schweitzer, C. T.; D'Agostino, C. *Inorg. Chem.* **1994**, *33*, 6278.

(25) Bautista, M.; Capellani, E. P.; Drouin, S. D.; Morris, R. M.; Schweitzer, C. T.; Sella, A.; Zubkowski, J. *J. Am. Chem. Soc.* **1991**, *113*, 4876.

Scheme 1

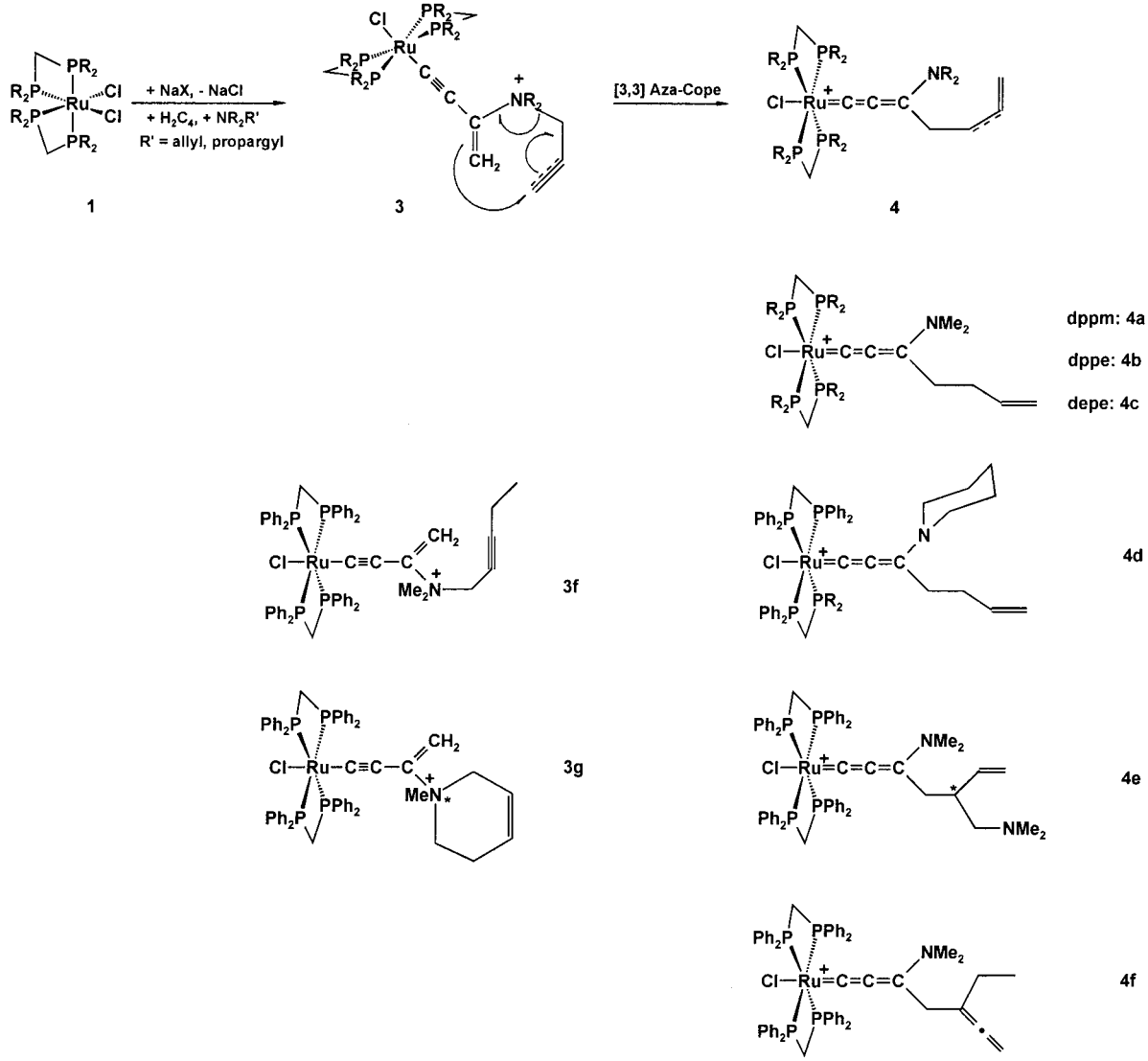

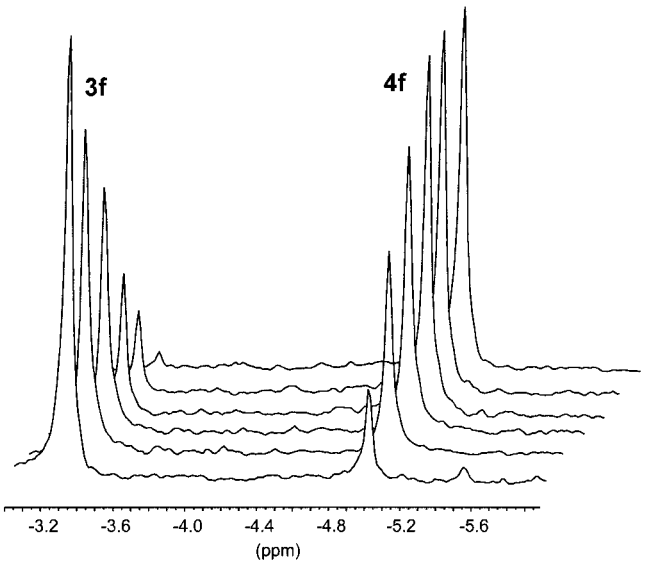

Figure 1. ^{31}P NMR spectra recorded during the rearrangement of **3f** to **4f** at 353 K.

Spectroscopy. Complexes **3f**,**g** exhibit the spectroscopic features that we already established for this class of compounds.[13a,d] Of special diagnostic value are the medium-intensity IR stretch of the modified alkynyl ligand at ca. 2035 cm^{-1} and the two doublet signals for the olefinic methylene protons at about δ 3.9 and 4.7 ppm with a geminal coupling of 3 Hz in the ^{1}H NMR spectrum. The resonance signals of the carbon atoms of the unsaturated C_4 chain appear at ca. 146−148 ppm as a quintet with a P−C coupling constant of 14 Hz (C_1), a singlet at ca. 108 ppm for C_4, and a broad signal at ca. 55 ppm assigned to the nitrogen-substituted C_3. C_2 is observed as a broad, unresolved signal for **3f** at δ 98.5 ppm but appears as a well-resolved quintet with J_{P-C} = 1.84 Hz at δ 95.7 ppm for the tetrahydropyridine derivative **3g**. The signals of the additional alkynyl and olefinic carbons in the ammonium side chain are readily identified by appropriate DEPT experiments at δ 68 and 94 ppm (C≡C, **3f**) and δ 120 and 125 ppm (HC═CH, **3g**).

To adequately describe the bonding within aminoallenylidene complexes, two different resonance forms have to be invoked, as illustrated in the Chart 1: the true cumulene type structure **A** and the alkynyl type resonance form **B**. The relative contribution of each individual resonance forms depends, inter alia, on the nature of the heteroatom and its ability to support a

Chart 1

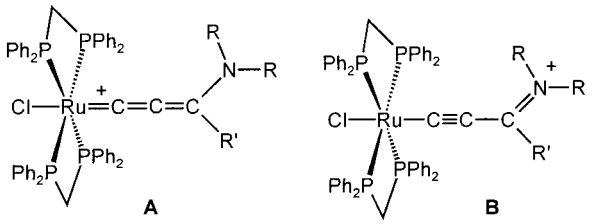

positive charge.[13c] In comparison to other substituents ER_n (E = C, n = 3; E = N, n = 2; E = O, S, Se, n = 1), nitrogen has special donor qualities, enhancing the importance of the iminiumalkynyl resonance form **B**. Substantial contributions of iminium type resonance forms are frequently invoked whenever electron-rich amino groups are in resonance with M=C double bonds such as in aminocarbene complexes,[30] aminoallenylidene complexes as their "cumulogous" counterparts,[13a,d,27−29] amino-substituted vinylcarbene complexes $[Cp(CO)(P^iPr_3)Ru{=}C(NRR')CH{=}CPh_2]^+$ (which, in fact, are more adequately described as the 1-azoniabutadienyl complexes $[Cp(CO)(P^iPr_3)Ru{-}C(=NRR')CH{=}CPh_2]^+$),[31] or 4-amino-1-metalla-1,3,5-trienes.[32] As will be detailed below, our aminoallenylidene complexes closely adhere to these expectations.

IR spectra of aminoallenylidene complexes **4** display an intense CC stretch at ca. 1980−2005 cm^{-1}. This band is at an intermediate position between Ru−alkynyl complexes of the same architecture[33,34] ($\nu_{C\equiv C}$ = 2045−2090 cm^{-1} with a tendency toward lower values for more electron withdrawing alkynes) and all-carbon-substituted Ru−allenylidene complexes, where this band occurs at 1920−1950 cm^{-1}.[26b,27] This argument requires that in both instances the band arises from the same C^1C^2 stretching mode such that the frequency truly provides a measure for the CC bond order at this position. Despite some caveats, this is qualitatively correct for the alkynyl complexes.[33] Our DFT calculations (vide infra) indicate that this also holds for amino-substituted allenylidene complexes **4**. Within the series of the dimethylallylamine-derived complexes **4a**−**c** there is a clear trend to lower ν_{CC} values as the electron richness of the ruthenium center increases (**4b**, 2005 cm^{-1}; **4a**, 1995 cm^{-1}; **4c**, 1979 cm^{-1}).[35] This is in line with a higher contribution of the cumulenic resonance form with the positive charge on the metal (and hence a stronger back-bonding to the electron-accepting allenylidene ligand) as the metal center becomes increasingly electron rich.[20b,c] Further indication as to the relevance of the iminiumalkynyl type resonance form **B** (Chart 1) comes from the observation of an intense C=N band near 1550 cm^{-1}, the assignment being again supported by theory. Similar bands in the range of 1500−1600 cm^{-1} were reported for the 1-azoniabutadienyl complexes $[Cp(CO)(P^iPr_3)Ru{-}C(=NRR')CH{=}CPh_2]^+$ [31] and, although not explicitly assigned there, for neutral aminoallenylidene complexes of chromium.[29b,c]

The ^{13}C shifts for the unsaturated carbon ligands follow the usual trend $\delta(C_1) > \delta(C_3) > \delta(C_2)$[13a,c,26−29] with $\delta(C_1)$ = 202−204 ppm, $\delta(C_3)$ = 154−157 ppm, and $\delta(C_2)$ = 119−122 ppm for the dppm derived complexes **4a**,**d**,**f**. Substitution of dppm by other diphosphine chelate ligands as in **4b**,**c** has hardly any influence on the remote β- and γ-carbons but shifts C_α by about 10 ppm upfield or downfield with respect to **4a**, with the depe-derived complex **4c** showing the signal at lowest field. The NMe_2 substituents of complexes **4a**−**f** give rise to two different resonance signals at 40−44 ppm, separated by ca. 3 ppm for each individual compound. Likewise, in their ^1H NMR spectra two distinct singlets are observed for the NMe protons. For the aliphatic depe derivative **4c** these signals appear at 3.18 and 3.28 ppm and are thus at rather similar field, whereas in complexes of phenyl-substituted diphosphine ligands shift differences of some 0.8 ppm are observed for each individual representative. One of these signals is shifted to remarkably high field (2.02−2.21 ppm). We attribute this signal to the methyl group which points toward the $ClRu(L_2)_2$ moiety. This brings these methyl protons proximate to the center of the arene ring. At this location the field induced by the diamagnetic ring current is antiparallel to the outer field, which accounts for the stronger shielding and for the anomalous high-field shift.

Two separate signals for the N-bound substituents point to hindered rotation around the C=N linkage, which must consequently be attributed to some fair degree of double-bond character, consistent with the iminium alkynyl resonance form **B** (see Chart 1). In fact, the rotational barrier is rather substantial, as shown by dynamic NMR investigations. Even at 363 K in CD_3NO_2 **4a**,**c**,**f** reveal no broadening of any of these signals. From the shift differences, values of 72 kJ/mol (**4a**,**f**) and 76 kJ/mol (**4c**) can be derived as conservative estimates for the lower limit for ΔG^*.

(26) (a) Touchard, D.; Pirio, N.; Fettouhi, M.; Ouahab, L.; Dixneuf, P. H. *Organometallics* **1995**, *14*, 5263. (b) Touchard, D.; Pirio, N.; Dixneuf, P. H. *Organometallics* **1995**, *14*, 4920. (c) Werner, H.; Stark, A.; Steinert, P.; Grünwald, C.; Wolf, J. *Chem. Ber.* **1995**, *128*, 49.

(27) Bruce, M. I. *Chem. Rev.* **1998**, *98*, 2797 and references therein.

(28) (a) Romero, A.; Peron, D.; Dixneuf, P. H. *J. Chem. Soc., Chem. Commun.* **1990**, 1410. (b) Peron, D.; Romero, A.; Dixneuf, P. H. *Gazz. Chim. Ital.* **1994**, *124*, 497.

(29) (a) Roth, G.; Fischer, H. *Organometallics* **1996**, *15*, 1139. (b) Stein, F.; Duetsch, M.; Pohl, E.; Herbst-Irmer, R.; de Meijere, A. *Organometallics* **1993**, *12*, 2556. (c) Duetsch, M.; Stein, F.; Lackmann, R.; Pohl, E.; Herbst-Irmer, R.; de Meijere, A. *Chem. Ber.* **1992**, *125*, 2051. (d) Aumann, R.; Jasper, B.; Rröhlich, R. *Organometallics* **1995**, *14*, 3173.

(30) (a) Fischer, E. O.; Heckl, B.; Werner, H. *J. Organomet. Chem.* **1971**, *28*, 359. (b) Fischer, E. O.; Leupold, M. *Chem. Ber.* **1972**, *105*, 599. (c) Boland-Lussier, B. E.; Hughes, R. P. *Organometallics* **1982**, *1*, 635. (d) Bianchini, C.; Masi, D.; Romerosa, A.; Zanobini, F.; Peruzzini, M. *Organometallics* **1999**, *18*, 2376.

(31) Bernard, D. J.; Esteruelas, M. A.; López, A. M.; Modrego, J.; Puerta, M. C.; Valerga, P. *Organometallics* **1999**, *18*, 4995.

(32) Barluenga, J.; Aznar, F.; Gutiérrez, I.; Martín, A.; García-Granda, S.; Lloraca-Baragaño, M. A. *J. Am. Chem. Soc.* **2000**, *122*, 1314.

(33) Manna, J.; John, K. D.; Hopkins, M. D. *Adv. Organomet. Chem.* **1995**, *38*, 79.

(34) (a) Hodge, A. J.; Ingham, S. L.; Kakkar, A. K.; Khan, M. S.; Lewis, J.; Long, N. J.; Parker, D. G.; Raithby, P. R. *J. Organomet. Chem.* **1995**, *488*, 205. (b) McDonagh, A. M.; Whittall, I. R.; Humphrey, M. G.; Skelton, B. W.; White, A. H. *J. Organomet. Chem.* **1996**, *519*, 229. (c) McDonagh, A. M.; Cifuentes, M. P.; Whittall, I. R.; Humphrey, M. G.; Samoc, M.; Luther-Davies, B.; Hockless, D. C. R. *J. Organomet. Chem.* **1996**, *526*, 99. (d) Whittall, I. R.; Humphrey, M. G.; Houbrechts, S.; Maes, J.; Persoons, A.; Schmid, S. M.; Hockless, D. C. R. *J. Organomet. Chem.* **1997**, *544*, 277.

(35) The basicity differences between the all-phenyl-substituted dppm and dppe ligands largely rely on the large differences in angular strain of their chelate complexes as imposed by the ligand backbone: Szczepura, L. F.; Giambra, J.; See, R. F.; Lawson, H.; Janik, T. S.; Jircitano, A. J.; Churchill, M. R.; Takeuchi, K. J. *Inorg. Chim. Acta* **1995**, *239*, 77.

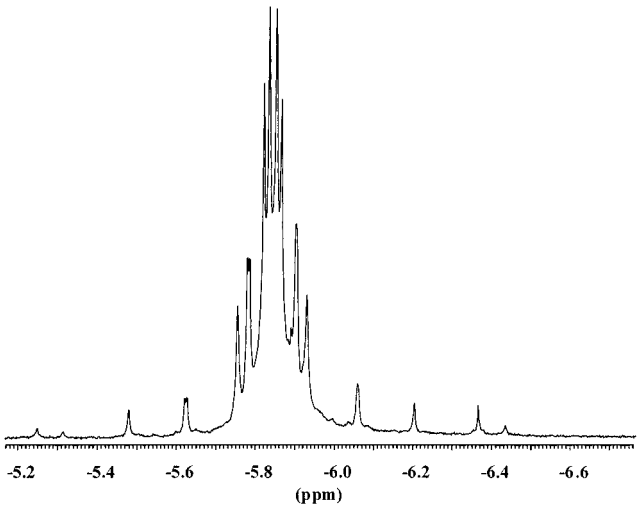

Figure 2. ^{31}P NMR spectrum of complex **3g**.

Other ^{13}C resonances of interest include the olefinic carbon atoms of the butenyl side chain that appear near δ 116 ppm (=CH_2) and δ 135 ppm (=CH). The allenyl substituent of **4f** gives rise to signals at δ 79.8 and 100.0 ppm for the outer carbon atoms and δ 204.3 ppm for the internal carbon atoms. The ^{31}P NMR spectra of complexes **4e** and **3g** are remarkable in that AA′BB′ multiplets are observed instead of a singlet normally associated with this architecture (Figure 2). This can be traced to the presence of a chirality center residing on either the allylic carbon of the butenyl side chain (**4e**) or the quaternary nitrogen (**3g**).

The UV/vis spectra display, besides the n/π^* and π/π^* transitions of the phosphine ligands, four different transitions: one broad band of rather low absorptivity ($\log \epsilon < 3$) at 620−690 nm, one shoulder at 435−465 nm with $\log \epsilon \approx 3$, one very intense absorption ($\log \epsilon > 4$) at ca. 400 nm, and another moderately intense band at ca. 265 nm, superimposed as a shoulder onto the even more intense phenylphosphine-based transitions in the case of the dppm- and dppe-derived complexes but clearly visible as an isolated band at 287 nm ($\log \epsilon = 3.06$) for the depe derivative **4c** (Figure 3). Comparison of the band positions in CH_2Cl_2 and CH_3CN reveals negative solvatochromism for the main absoption band with $\Delta\nu$ ranging from 600 to 710 cm^{-1}, indicating a decrease in polarity upon electronic excitation. There is again a marked influence of the metal center on the band positions, mainly on the two low-energy bands which are associated with the symmetry-forbidden HOMO/LUMO transition and the symmetry-allowed excitation from the second highest occupied level (SHOMO), as will be detailed in a later section. The HOMO/LUMO and the SHOMO/LUMO transition energies steadily decrease within the series **4b** > **4a** > **4c** from 16 000 to 14 500 and from 25 700 to 25 000 cm^{-1}. This mirrors the trend in ^{13}C NMR shifts for the carbon atom C_α. It is generally agreed that the characteristic low-field shifts of carbene, vinylidene, and allenylidene carbon atoms arise from the paramagnetic term which, inter alia, depends on the energy gap between occupied and unoccupied levels to which the carbon atom in question contributes.[36] The lower the energy gap, the more downfield the resonance signal. For a series of compounds so closely related as **4a**−**c**, one may reasonably expect other factors such as the p-orbital contributions to both levels and the symmetry properties of the transitions in question to be constant such that the energy gap becomes the determining factor.

Crystallography. The molecular structure of complex **4a** has been communicated in our previous report.[13a] We have also characterized the dppe analogue **4b**, which crystallizes as a tris(dichloromethane) solvate. Figure 4 gives a graphical representation of the cation. Selected bond distances and angles of the cationic aminoallenylidene complexes **4a**,**b** are provided in Table 1, while all information pertinent to data collection and refinement for **4b** are collected in Table 2. Apart from the widely differing cisoid P−Ru−P angles due to the constraints imposed by the chelate ligand backbone, the cation structures are very similar. The whole $ClRuC_3(CH_3)N$ entity is essentially coplanar (maxmium deviation 0.096 Å for C3) and almost perpendicular to the best plane RuP_4 (interplanar angle 89.3°). The RuC_3 axis is nearly linear for both cations (**4a**,**b**: Ru−C1−C2 = 175.3(4), 177.8(7)°; C1−C2−C3 = 175.1(6), 168.7(9)°), with some higher degree of bending at C2.

From a structural viewpoint one may reasonably expect that a higher contribution of the alkynyl type resonance form should lead to shorter C1−C2 but longer Ru−C1 and C2−C3 bond lengths as compared to the cumulenic structure. **4a**,**b** may therefore be compared with Ru(II)−alkynyl complexes on one hand and all-carbon-substituted allenylidene complexes, which better, but still not perfectly, resemble the genuine cumulenic structure[26] on the other. In fact, there is a substantial bond length alternation along the RuC_3N chain. The Ru−C1 bond lengths in **4a**,**b** (1.950(4) and 1.934(8) Å) are considerably shorter than those in ruthenium alkynyl complexes (1.994−2.078 Å),[27,33,37] a notable exception being *trans*-$Cl(dppm)_2RuCCH$, for which a short Ru−C bond of 1.906(9) Å and a short C≡C bond of 1.162(9) Å have been reported.[38] They are, however, longer than those in all-carbon-substituted allenylidene complexes of the same or closely related ruthenium(II) fragments (1.85−1.886 Å).[27] The same trend holds for the C1−C2 interatomic distances. The observed values of 1.218(6) Å in **4a** and 1.203 Å in **4b** are only slightly long with respect to the C≡C triple bond in purely organic compounds (1.189 Å for the C≡C bond in alkynes, where the sp carbon is conjugated with sp^2 carbon atoms)[39] or those in complexes of σ-bonded alkynyl ligands, for which an average value of 1.201 Å has been determined for a broad range of

(36) Czech, P. T.; Ye, X.-Q.; Fenske, R. F. *Organometallics* **1990**, *9*, 2016.

(37) (a) Field, L. D.; George, A. V.; Hockless, D. C. R.; Purches, G. R.; White, A. H. *J. Chem. Soc., Dalton Trans.* **1996**, 2011. (b) Hodge, A. J.; Ingham, S. L.; Kakkar, A. K.; Khan, M. S.; Lewis, J.; Long, N. J.; Parker, D. G.; Raithby, P. R. *J. Organomet. Chem.* **1995**, *488*, 205. (c) McDonagh, A. M.; Whittall, I. R.; Humphrey, M. G.; Skelton, B. W.; White, A. H. *J. Organomet. Chem.* **1996**, *519*, 229. (d) McDonagh, A. M.; Whittall, I. R.; Humphrey, M. G.; Hockless, D. C. R.; Skelton, B. W.; White, A. H. *J. Organomet. Chem.* **1996**, *523*, 33. (e) McDonagh, A. M.; Cifuentes, M. P.; Whittall, I. R.; Humphrey, M. G.; Samoc, M.; Luther-Davies, B. *J. Organomet. Chem.* **1996**, *526*, 99. (f) Zhu, Y.; Millet, D. B.; Wolf, M. O.; Rettig, S. J. *Organometallics* **1999**, *18*, 1930. (g) McDonagh, A. M.; Lucas, N. T.; Cifuentes, M. P.; Humphrey, M. G.; Houbrechts, S.; Persoons, A. *J. Organomet. Chem.* **2000**, *605*, 193.

(38) Haquette, P.; Pirio, N.; Touchard, D.; Toupet, L.; Dixneuf, P. H. *J. Chem. Soc., Chem. Commun.* **1993**, 163.

(39) Lide, D. R.; Frederikse, H. P. R. *CRC Handbook of Chemistry and Physics*, 76th ed.; CRC Press: Boca Raton, FL, 1995.

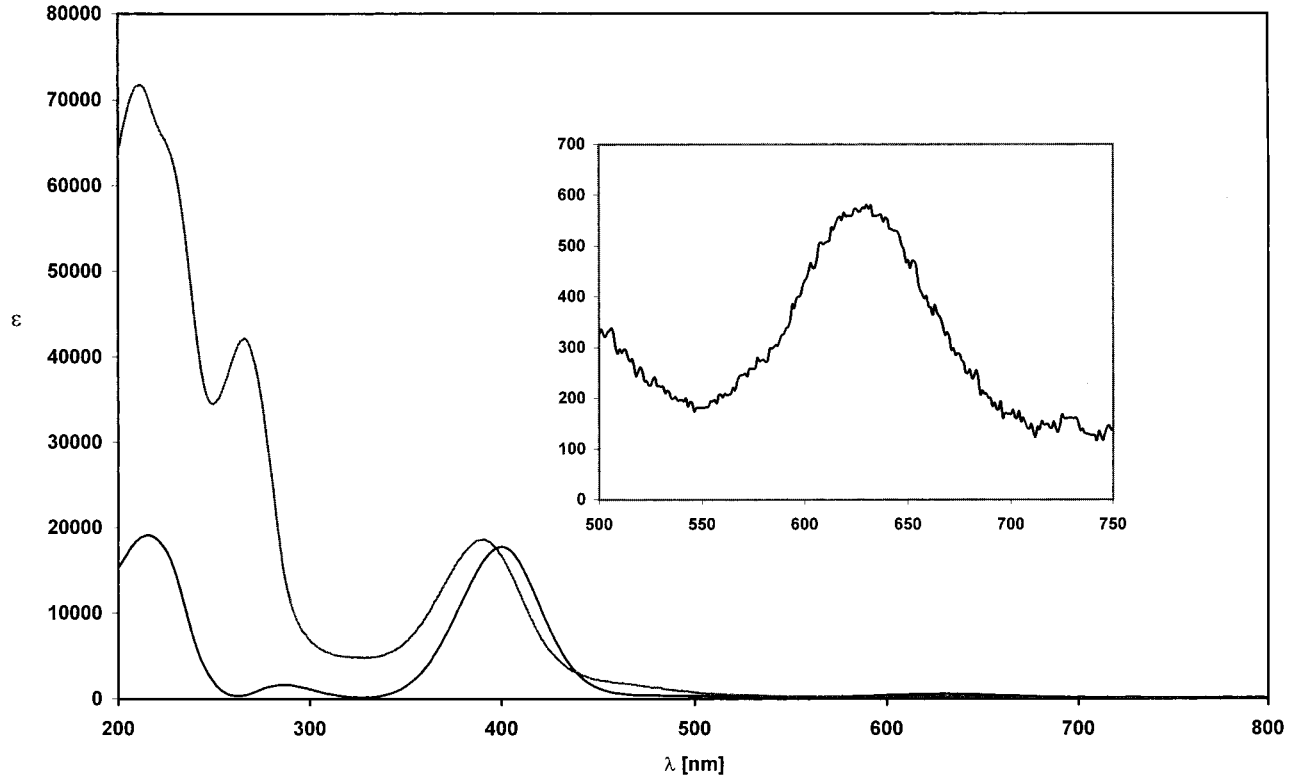

Figure 3. UV/vis spectra of aminoallenylidene complexes **4c,d** in CH_3CN. Insert: 500−750 nm region for complex **4c** magnified.

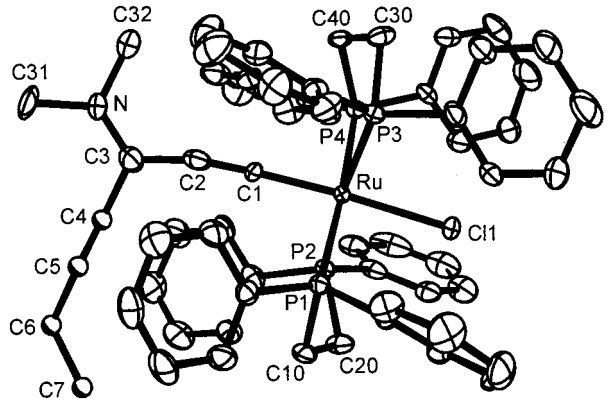

Figure 4. Plot of the cation *trans*-$[Cl(dppe)_2RuCCC(NMe_2)(C_4H_7)]^+$ of complex **4b** with the atomic labeling scheme of the more important atoms.

transition metals.[33] In neutral mono- or bis(alkynyl) complexes of the *trans*-$XRu(L_2)_2$ fragment, values are typically in the range of 1.190−1.226 Å (average value 1.203 Å).[37] In cationic all-carbon-substituted allenylidene complexes $[\{Ru\}=C=C=CRR']^+$ there seems to be a tendency toward longer CC bonds (1.218(6)−1.29(3) Å, average 1.259 Å).[27] The C2−C3 bond lengths of 1.372(9) Å (**4a**) and 1.393(13) Å (**4b**) are roughly midway between those for a single bond between an sp- and an sp^2-hybridized carbon atom (1.431 Å) and a C=C double bond in allenes (1.307 Å)[39] but fall within the range observed for all-carbon-substituted allenylidene complexes of the same metal fragments (1.329−1.42 Å).[27] The most revealing part of the structure is, however, the immediate surroundings of the nitrogen atom. Thus, the N−C3 bond lengths in **4a**,**b** are much shorter than the *N*-methyl bonds (1.313(13) Å vs 1.460(11) and 1.466(13) Å in **4b**; comparable bonds in **4a** may be artificially short and long due to disorder of the whole C3−N−C10,C11 butenyl entity). Moreover, the angle sum at nitrogen is exactly 360°, such that the nitrogen clearly has iminium character. This feature seems to be general for all structurally characterized aminoallenylidene complexes irrespective of the exact nature of the metal fragment.[12b,13a,29b,d,40]

In conclusion, structural and spectroscopic data for aminoallenylidene complexes **4** agree well in placing

Table 1. Selected Bond Lengths (Å) and Angles (deg) for $[Cl(L_2)_2RuCCC(NMe_2)C_4H_7]^+EF_6^-$ (L_2 = dppm, E = P, 4a; L_2 = dppe, E = Sb, 4b)

	4a	4b
	Bond Lengths[a]	
Ru−Cl1	2.4686(10)	2.457(2)
Ru−P1	2.3651(11)	2.394(2)
Ru−P2	2.3733(11)	2.392(2)
Ru−P3	2.3521(11)	2.411(2)
Ru−P4	2.3570(11)	2.396(2)
Ru−C1	1.950(4)	1.934(8)
C1−C2	1.218(6)	1.232(13)
C2−C3	1.372(9)	1.393(13)
N−C3	1.244(8)	1.320(13)
C31−N	1.505(7)	1.460(11)
C32−N	1.495(6)	1.466(13)
C3−C4	1.499(7)	1.48(2)
C4−C5	1.470(8)	1.52(4)
C5−C6	1.499(9)	1.56(4)
C6−C7	1.317(9)	1.34(5)
	Bond Angles (deg)	
P1−Ru−P2	70.73(4)	83.02(7)
P3−Ru−P4	71.62(4)	82.67(8)
P3−Ru−P1	108.21(4)	97.82(6)
P4−Ru−P2	109.88(4)	96.92(6)
C1−Ru−Cl1	175.21(12)	176.8(2)
C2−C1−Ru	175.3(4)	177.8(7)
C1−C2−C3	175.1(6)	168.7(9)
C2−C3−N	126.6(7)	123.1(8)

[a] For the disordered atoms C3, N, C31, C4−C7 (**4a**) and C4−C7 (**4b**) only the major orientation is given.

Table 2. Crystallographic Data for Complex 4b

formula	$C_{61}H_{61}ClF_6NP_4RuSb\cdot 3CH_2Cl_2$
fw	1559.04
temp	173(2) K
wavelength	0.71073 Å
cryst syst	monoclinic
space group	*Ia*
a	19.162(2) Å
b	16.458(2) Å
c	22.685(4) Å
β	112.51(8)°
V	6608.9(2) Å^3
Z	4
density (calcd)	1.567 Mg/m^3
absorption coeff	1.074 mm^{-1}
F(000)	3144
cryst size	0.3 × 0.25 × 0.15 mm
θ range for data collection	1.57−27.51°
index ranges for data collection	$-22 \le h \le 24$, $-13 \le k \le 21$, $-24 \le l \le 29$
no. of rflns msd	8046
no. of indep rflns	7775 (R(int) = 0.0518)
refinement method	full-matrix least squares on F^2
no. of data/restraints/params	7775/11/757
goodness of fit on F^2	1.056
final *R* indices ($I > 4\sigma(I)$)	R1 = 0.0505, wR2 = 0.1332
R indices (all data)	R1 = 0.0619, wR2 = 0.1414
absolute structure param	0.62(4)
largest diff peak and hole	1.59 and −1.04 e/Å^3

Table 3. Electrochemistry Data for Complexes 4a−f and 3f,g

compd	solvent	$E_{1/2}$(ox) (V)	$E_{1/2}$(red) (V)	E_{follow} (V)
4a	CH_2Cl_2	+0.57	−2.14[a,b,e]	
	THF	+0.50	−2.155[b,e]	−1.38,[d] −1.00,[d] 0.32
4b	CH_2Cl_2	+0.665	−2.11[a,b,e]	−1.425, −1.10[d]
4c	CH_2Cl_2	+0.425	<−2.20	
	THF	+0.325	−2.16[b,e]	
4d	CH_2Cl_2	+0.60[c]	−2.17[a,b,e]	−1.45,[d] +0.40
	CH_3CN	+0.595	−2.09[a,b,e]	−1.375[d]
4e	CH_2Cl_2	+0.645[a,e]	−2.11[a,e]	
4f	CH_2Cl_2	+0.57	−2.18[a,b,e]	−1.47,[d] −1.04,[d] +0.30
	THF	+0.57	−2.08[a,b,e]	
3f	CH_2Cl_2	+0.365[c]	nd[g]	
	CH_3CN	+0.375[c]	nd	
3g	CH_2Cl_2	+0.33[e]	nd	−0.43[d]
	THF	+0.28[e]	−2.67[d], −2.90[d]	−1.44,[d,f] −0.79,[d] +0.23,[d] +0.55

[a] $E_{1/2}$ determined at 195 K. [b] At 298 K; irreversible 2e$^-$ process. [c] Quasireversible. [d] Peak potentials of irrversible processes determined at v = 0.2 V/s. [e] Only partially reversible. [f] Cathodic peak following oxidation. [g] nd = not determined.

them at an intermediate position between "true" allenylidene and 1-azoniabutenynyl complexes with major contributions of the latter resonance form.

Electrochemistry. We have previously reported on the electrochemical behavior of ammoniobutenynyl complexes of type **3**.[13d] A combination of cyclic and square-wave voltammetry revealed partially to fully reversible one-electron oxidation to Ru(III) species and irreversible reductions occurring as two closely spaced waves. The reduction processes are accompanied by loss of the free amine, as was inferred from the distinct changes in the anodic response after scanning past the cathodic waves, identical with those imparted by the presence of the free amine. **3f**,**g** behave identically and present no new features. Relevant data are collected in Table 3. Half-wave potentials are reported relative to the internal ferrocene/ferrocenium standard throughout.

The electrochemical responses of aminoallenylidene complexes **4a**−**g** are all rather similar, irrespective of the substituents on the iminium nitrogen or the solvent used in the experiment. Each complex displays a chemically reversible one-electron oxidation, as ascertained by a peak current ratio $i_{p,rev}/i_{p,forw}$ of exactly or close to unity. In several instances the oxidation waves show the signatures of somewhat sluggish electron transfer kinetics, as is occasionally observed for Ru(II/III) couples in organometallic environments.[13d,41,42] Diagnostic values such as the peak-widths at half-height for the forward peak or the peak-to-peak separations progressively exceed those measured for the internal Nernstian ferrocene/ferrocenium standard when the sweep rate is increased or the temperature is lowered.[43] For the dppm-derived complexes **4a**,**d**,**f** the oxidation potential lies in a rather narrow region between +0.57 and +0.60 V. The only exception is complex **4e**, featuring a dangling amino group within the side chain. This species not only calls for higher sweep rates in order to suppress chemical decomposition following electron transfer but also exhibits a somewhat higher $E_{1/2}$ value of +0.645 V. The oxidation potentials are consistently more anodic than those for ammoniobutenynyl complexes **3**, which are usually in the range of +0.33 to +0.36 V in CH_2Cl_2 solution.[13d] The isomeric couple **3f**/**4f** clearly illustrates this point: **3f** is more easily oxidized by some 200 mV than its rearranged counterpart. This difference is attributed to the positive charge in resonance or even residing on the metal center in complexes **4**, while it is further removed from the metal center in ammoniobutenynyl complexes **3**. Such reasoning requires that the oxidation directly involves the metal center. We will later address this issue from a theoretical viewpoint.

All complexes **4** also undergo a single reduction process which shows, however, some peculiarity: at 298 K and low sweep rates v this process is chemically irreversible and its peak currents are approximately twice as high as that of the oxidation wave (Figure 5a). As the sweep rate is increased and/or the temperature lowered, the following chemical reaction is gradually suppressed such that the reverse peak for the reoxidation is observed. This allows for the evaluation of thermodynamically meaningful $E_{1/2}$ values for the reduction process (Figure 5b),[44] although full chemical reversibility can rarely be achieved. As the reversibility increases, the forward peak current for the reduction wave more and more resembles that of the oxidation. Similar results were obtained from the i vs $t^{-1/2}$ or i vs $t^{1/2}$ plots in chronoamperometry or chronocoulometry measurements on some individuals.[45] All this points to the electrochemically induced chemical degradation of the reduced species producing other electroactive species that are further reduced by one electron at the reduction potential of the parent complex. Indeed, several new features are observed upon scan reversal following reduction. While the absolute response depends on the nature of the solvent (see Table 3 for details), more

(40) Fischer, E. O.; Kalder, H. J.; Frank, A.; Köhler, H.; Huttner, G. *Angew. Chem.* **1976**, *88*, 683; *Angew. Chem., Int. Ed. Engl.* **1976**, *15*, 623.

(41) Winter, R. F.; Scheiring, T. *Z. Anorg. Allg. Chem.* **2000**, *626*, 1196.

(42) al Dulaimi, J. P.; Clark, R. J. H.; Saavedra, M. S.; Salam, M. A. *Inorg. Chim. Acta* **2000**, *300*−*302*, 175.

(43) Nicholson, R. S. *Anal. Chem.* **1965**, *37*, 1351.

(44) Nicholson, R. S.; Shain, I. *Anal. Chem.* **1964**, *37*, 706.

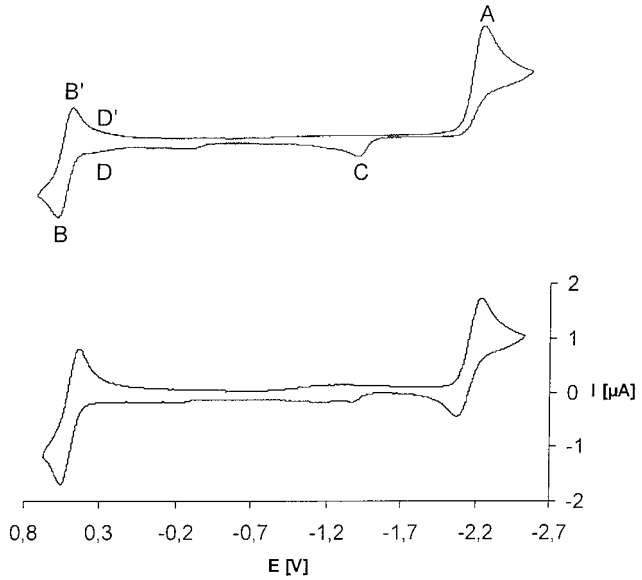

Figure 5. Cyclic voltammograms of complex **4a** in THF solvent at (a, top) 298 K and $v = 0.2$ V/s and (b, bottom) 195 K and $v = 0.1$ V/s.

common features include an irreversible anodic peak at ca. −1.37 to −1.45 V (peak C in Figure 5b) and a more or less reversible couple at ca. +0.32 to +0.40 V: i.e., sligthly cathodic of the oxidation wave (peaks D and D′). Since the species responsible for this wave are only generated when the reduction is performed first and much of this species is lost by diffusion into the bulk of solution during the reverse scan (note that the potential difference between this feature and the reduction potential exceeds 2 V), the peak heights are very small. Therefore, peaks D and D′ appear only as shoulders superimposed on the original oxidation wave, peaks B and B′. All waves of electrogenerated species gradually disappear as the reduction becomes more reversible.

Electrochemical half-wave potentials provide an even more direct measure for the electron density on the metal fragment, providing the actual redox process deeply involves the metal. Our data point in this direction: as the electron donation of the diphosphine ligands increases, the $E_{1/2}$ values of both the oxidation *and* the reduction processes experience a cathodic shift. From our admittedly limited data set the effect on the oxidation potential seems to exceed that on the reduction, and this may reflect a higher metal contribution to the HOMO as compared to the LUMO. This is indeed found in our calculations (vide infra).

Spectroelectrochemistry. With their characteristic C≡C and C═N IR bands and their charge-transfer absorption in the visible region aminoallenylidene complexes *trans*-$[Cl(L_2)_2RuCCC(NR_2)R']^+$ (**4**) possess highly intense spectroscopic labels that are sensitive toward the spin and charge distribution within the molecule. Since most representatives are reversibly oxidized to their respective dications, combining electrochemistry with various spectroscopic techniques should allow us to probe for the effect of electron transfer upon the bonding and the structure. We were able to record the UV/vis and IR spectra of the oxidized dications for complexes **4a**,**c**,**d**,**f** and the EPR spectra of the oxidized forms of complexes **4a**,**d** generated directly in the EPR tube. The results of the UV/vis and IR spectroelectrochemical experiments are summarized in Table 4. In each case we checked for chemical reversibility by rereducing the oxidized forms to the parent compounds. In general, the optical yield of the starting material was higher than 85% for optical and higher than 75% for the IR methods, the differences being due to the higher concentrations (and the concomitant longer electrolysis times) required in IR spectroscopy. In every case rereduced samples displayed in the spectral region of interest no features other than those of the parent material, such that we feel confident that the traces obtained after exhaustive oxidation really originate from the oxidized species.

Figure 6 documents the changes in the optical spectra during the oxidation of compounds **4c**,**d**. Most striking is a blue shift of the prominent absorption band by about 4300 cm^{-1} upon oxidation. A plausible explanation is the preferential lowering of the occupied level (which in this instance is the second highest occupied molecular orbital (SHOMO), as will be discussed later) with respect to the LUMO upon oxidation, provided that the origin of this band remains unaffected by the electron-transfer process. The similar extinction coefficients in both oxidation states agree favorably with this assumption. We have already reported a shift of identical magnitude of this band during the *second* oxidation of the aminoallenylidene complex *trans*-$[Cl(dppm)_2RuCCC(NMe_2)C_2H_4Fc]^+$, where the appended ferrocenyl moiety (Fc) is oxidized first.[13b] The HOMO/LUMO band located at 630−650 nm also shifts during oxidation and is then observed as a much stronger band at ca. 2000 cm^{-1} lower energy. Again, this has precedent in the ferrrocenylethyl-substituted analogue.[13b] This new band was tentatively assigned to a d−d transition within the d^5 configuration of Ru(III) but, in light of our theoretical results (vide infra), involves the metal and the unsaturated ligand and displays considerable charge-transfer characteristics.

In IR spectroelectrochemistry the highly intense allenylidene stretch bleaches during oxidation and is replaced by a new band at 1950−1920 cm^{-1}, as shown for the allylpiperidine-derived complex **4d** in Figure 7. This feature is so weak that high concentrations up to the upper detection limit of the IR spectrometer are mandatory in order to observe it. We wish to emphasize again that the largely reduced absorptivity of this feature is an intrinsic property of our systems and is not due to extensive decomposition, as ascertained by back-electrolysis. In contrast to the C≡C stretch, the C═N band retains its absorptivity while also being shifted upon oxidation. The direction of this shift is, however, not uniform. A lowering of the C═N frequen-

(45) In chronoamperometry, the diffusional current is given by the Cottrell equation $i = nFAD^{1/2}c/(\pi t)^{1/2}$, n being the number of electrons involved, A the active electrode area, F the Faraday constant, D the diffusion constant of the analyte, and c the analyte concentration. Plots of i vs $t^{-1/2}$ give a straight line. From its slope D can be determined once n is known. For **4e**, D values of 0.62×10^{-5} and 0.14×10^{-5} cm^2 s^{-1} were determined in 0.25 mM NBu_4PF_6 in CH_2Cl_2 at 298 and 215 K, respectively, on the basis of the oxidation. If the analyte undergoes two different electron-transfer processes, the ratio of the slopes equals the ratio of electrons transferred in these steps, provided the measurements are performed under identical experimental conditions. See also: Bard, A. J.; Faulkner, L. R. *Electrochemical Methods: Fundamentals and Applications*; Wiley: New York, 1980; Chapter 5.9.

Table 4. Spectroelectrochemical Results on Complexes 4

		prior to oxidn		after oxidn[b]	
compd	solvent[a]	λ_{max} (nm) (ϵ (mol^{-1} cm^{-1}))	ν (cm^{-1})	λ_{max} (nm) (ϵ (mol^{-1} cm^{-1}))	ν (cm^{-1})
4a	DCE	640 (310) 396 (16 800)	1995 (vs, CC) 1572 (s, CN)	567 (940) 402 (sh) (4300) 338 (16 800)	1948 (w, CC) 1554 (s, CN)
4c	CH_3CN	630 (380) 400 (17 400) 287 (1150)	1979 (vs, CC) 1564 (s, CN)	557 (1020) 396 (sh, 6300) 341 (12 700) 284 (6100)	nd[c] 1532 (s, CN)
4d	DCE	654 (150) 395 (21 500) 268 (49 000)	1990 (vs, CC) 1547 (s, CN)	567 (1400) 339 (10 850) 288 (25 600) 277 (24 500)	1942 (w, CC) 1590 (s, CN)
4f	DCE	628 (630) 400 (11 800) 264 (32 500)	1997 (vs, CC) 1927 (m, CC) 1573 (s, CN)	571 (1500) 403 (sh) (5100) 340 (9150)	1919 (vw, CC) 1545 (s, CN)

[a] DCE = 1,2-$Cl_2C_2H_4$. [b] ϵ values of oxidized species represent lower limits because of some decomposition during oxidation. [c] nd = not determined.

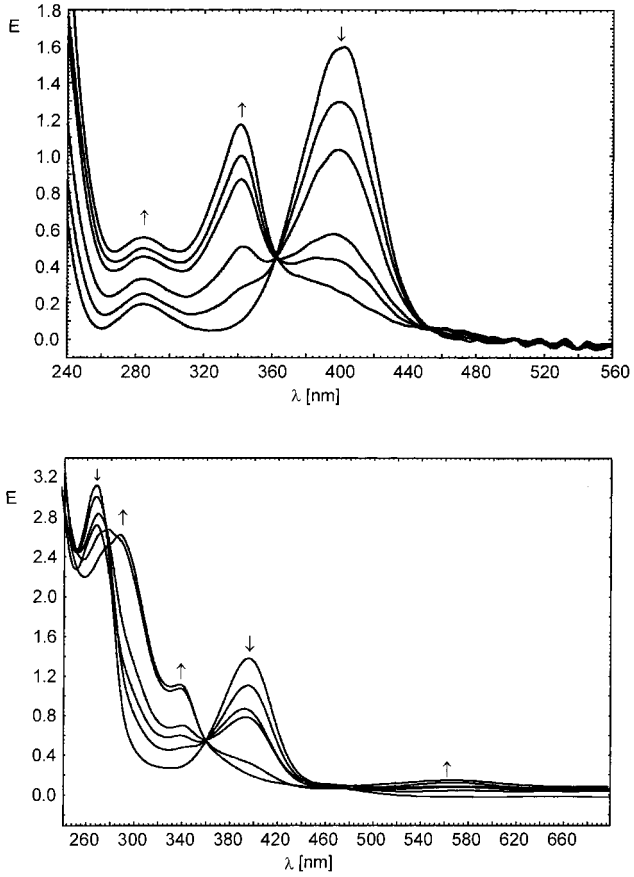

Figure 6. UV/vis spectra recorded during the anodic oxidation of (a, top) compound **4c** and (b, bottom) compound **4d** in an OTTLE cell.

cies is observed for complexes where the iminium nitrogen is substituted by two methyl groups, while the frequency increases for **4d**, where the iminium nitrogen is part of a saturated six-membered ring.

The most conclusive result as to the oxidation site within complexes **4** is expected from EPR spectroscopy. At 95 K oxidized samples display rhombic patterns with considerable spread of the individual g components and average g values far removed from that of the free electron, indicating a primarily metal-centered oxidation (**4c**, $g_x = 2.400$, $g_y = 2.067$, $g_z = 1.888$, $g_{av} = 2.118$; **4f**, $g_x = 2.135$, $g_y = 2.022$, $g_z = 1.999$, $g_{av} = 2.052$). Upon thawing, EPR activity is reversibly lost.

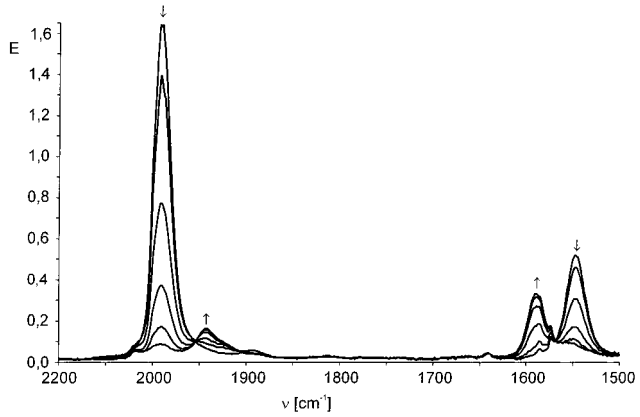

Figure 7. IR spectra recorded during the anodic oxidation of compound **4c** in an OTTLE cell.

Theoretical Calculations. At this point we felt it highly desirable to augment our experimental studies with theoretical calculations. To restrict computational time to a reasonable limit, these were performed on simplified models by replacing the chelating phenyl- or ethyl substituted diphosphine ligands by PH_3 and introducing a methyl substituent on the terminal carbon instead of the actual ones in complexes **4a**−**f**. While the latter simplification is expected to have only very minor effects, phosphine substitution certainly has a larger influence due to the differences in electronic properties and PRuP angles[4b] between the model and our real systems.

(a) The Butatrienylidene Intermediate. While this work was in progress, an exhaustive investigation on cumulene complexes $(CO)_5Cr{=}C_n{=}CH_2$ ($n = 1-9$) on essentially the same theoretical level was published, including the butatrienylidene analogue.[18] This provides us now with the opportunity to compare crucial parameters of the metallabutatrienylidene entities for d^6 metal fragments with vastly different electronic properties. Table 5 shows the G98/B3LYP and ADF/BP calculated bond lengths of the ruthenium model complex along with those of its $Cr(CO)_5$ analog[18] and the experimental structures of *trans*-$[Cl(dppe)_2RuC_5Ph_2]^{+}$ [11b] and of *trans*-$Cl(P^iPr_3)_2IrC_4Ph_2$, the only terminal butatrienylidene complex that has been structurally characterized to date.[9] The calculated bond lengths within the C_4H_2 fragment clearly indicate a cumulenic structure with only a slight progression toward the terminal CH_2

Table 5. Comparison of Calculated Bond Lengths of $[RuCl(PH_3)_4C_4H_2]^+$ with Those for $(CO)_5CrC_4H_2$[18] and the Experimental Structures of *trans*-$[Cl(dppe)_2RuC_5Ph_2]^+$[11b] and *trans*-$ClIr(P^iPr_3)_2C_5Ph_2$[9]

bond	calcd ADF/BP	calcd G98/ B3LYP	calcd[a] $(CO)_5CrC_4H_2$	$[Cl(dppe)_2RuC_5Ph_2]^+$	$ClIr(P^iPr_3)_2C_5Ph_2$
M−Cl	2.458	2.468		2.430(3)	2.356(2)
M−P	2.390	2.390		2.421 (av)	2.353 (av)
Ru−C1	1.886	1.886		1.891(9)	1.816(6)
C1−C2	1.282	1.282	1.279	1.25(1)	1.283(8)
C2−C3	1.290	1.297	1.285	1.30(1)	1.275(8)
C3−C4	1.309	1.309	1.309	1.39[b]	1.339(8)

[a] On the ADF/BP level. [b] Terminal C.

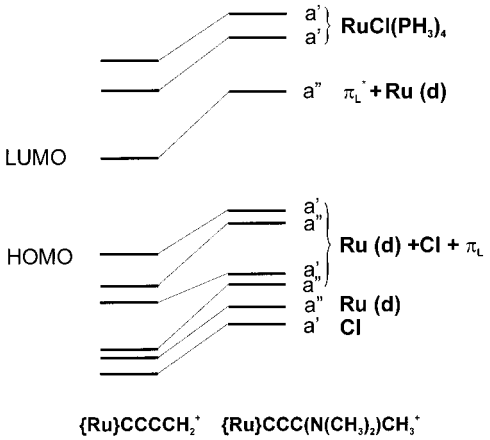

Figure 8. MO schemes for the butatrienylidene model complex $[Cl(PH_3)_4RuC_4H_2]^+$ (left) and the aminoallenylidene model complex $[Cl(PH_3)_4RuC_3\{N(CH_3)_2\}(CH_3)]$ (right).

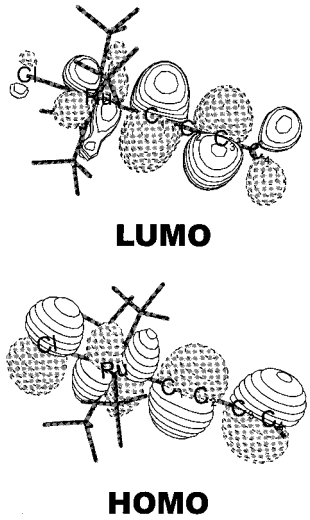

Figure 9. Graphic representations of the frontier orbitals of the butatrienylidene model complex $[Cl(PH_3)_4RuC_4H_2]^+$.

Table 6. ADF Calculated One-Electron Energies and Percentage Composition of Selected Highest Occupied and Lowest Unoccupied Molecular Orbitals of $[Cl(PH_3)_4RuC_4H_2]^+$ Expressed in Terms of Composing Fragments

MO	*E* (eV)	prevailing character	Ru	C_1	C_2	C_3	C_4	Cl
$10b_1$ occupied	−6.99	$\pi^* C_4H_2 + d_{Ru}$	17 (d)	34	3	35	1	2
$9b_2$	−8.48	$Ru + Cl + \pi^* C_4H_2$	30 (d)	6	16	2	20	22
$9b_1$	−9.10		12 (d)	2	2	5	1	73

group. Our data are virtually identical with those obtained by Sgamellotti et al. for the $Cr(CO)_5$ derivative and also favorably agree with the experimentally determined data with larger deviations for the terminal CC bond involving the substituted sp^2 center, as expected. The metrical parameters of the butatrienylidene ligand therefore appear to be rather insensitive to the electronic properties of the metal fragment to which it is attached.

A graphic representation of the MO scheme as calculated by the ADF/BP method is given on the left-hand side of Figure 8. As for the $Cr(CO)_5$ analogue of our model complex, the HOMO and the LUMO result from the interaction of the metal fragment (Cl, Ru, and P) with the occupied or unoccupied π-orbitals of the cumulene ligand, the HOMO being orthogonal and the LUMO parallel to the plane of the terminal CH_2 group. Plots of the frontier orbitals are provided as Figure 9, and the orbital composition is represented in Table 6, while the first row of Table 7 lists the atomic charges from Mulliken analysis. Our ruthenium intermediate follows the same pattern as that established for the $Cr(CO)_5$ complex: the HOMO is dominated by contributions from the metal (30% in our complex vs 39% for the Cr complex) and carbon atoms located at even positions within the C_4 chain (16% and 20% vs 16.5% and 19% for C_2 and C_4, respectively). The opposite holds for the LUMO: here the metal contributes significantly less (17% for our complex, 13% for the Cr system) while more than 70% arises from the cumulene ligand with dominant contributions from carbon atoms C_1 and C_3.

This has a direct bearing on the site of nucleophilic addition to the allenylidene ligand. In principle, the reactivity of our butatrienylidene intermediate could be charge or orbital controlled with either one single factor dominating or both being equally important contributors. Charge-controlled reactivity requires a significant charge accumulation on one specific center. As shown by Mulliken analysis (see Table 7), the charge differences are rather small, again paralleling the results on the $(CO)_5Cr$ system.[18] This points to orbital control. There remains, however, the question of why no addition to the carbon atom adjacent to the metal has been observed to date for butatrienylidene complexes even though the LUMO indicates a rather unselective addition to either C_1 or C_3. In fact, cationic allenylidene complexes may display both modes of reactivity, depending on the nature of the metal fragment and the entering nucleophile.[26a, 46−51] Addition to C_1 requires, however, a metal fragment of only limited steric bulk, offering at least one "open" side with a smaller size ligand for the approach of the incoming nucleophile (e.g. $\{(\eta^6\text{-arene})Ru(PR_3)Cl\}^+$,[50] $\{(\eta^5\text{-indenyl})Ru(PPh_3)(CO)\}^+$,[47c] and $\{CpRu(PPh_3)(CO)\}^+$ [35b,48e,f]). The only exception seemingly is $[(\eta^5\text{-indenyl})L_2Ru{=}C{=}C{=}CPhH]^+$ (L_2 =

(46) (a) Cadierno, V.; Gamasa, M. P.; Gimeno, J.; López-González, M. C.; Borge, J.; García-Granda, S. *Organometallics* **1997**, *16*, 4453. (b) Esteruelas, M. E.; Gómez, A. V.; Lahoz, F. J.; López, A. M.; Oñate, E.; Oro, L. A. *Organometallics* **1996**, *15*, 3423.

Table 7. ADF/BP Calculated Mulliken Charges within $[Cl(PH_3)_4RuC_3RR']^+$ Complexes

	charge on							
R/R′	Ru	C_1	C_2	C_3	R	R′	Cl	PH_3
CH_2/−	0.605	−0.251	−0.061	0.111	−0.074 (C)		−0.371	0.260
$N(CH_3)_2$/CH_3	0.836	−0.255	−0.265	−0.118	−0.128 (N)	−0.128 (C)	−0.420	0.120

Table 8. ADF-BP Calculated Bond Lengths for $[Ru(Cl)(PH_3)_4C_3CH_3N(CH_3)_2]^{n+}$

		exptl			
bond	calcd	**4a**	**4b**	calcd $^2A'$ state	calcd $^2A''$ state
Ru−Cl	2.470	2.469	2.457	2.364	2.376
Ru−P (av)	2.349	2.350	2.399	2.405	2.395
Ru−C1	1.957	1.950	1.934	1.951	1.971
C1−C2	1.256	1.218	1.232	1.257	1.251
C2−C3	1.379	1.372	1.393	1.394	1.402
C3−C4	1.504	1.499	1.48	1.500	1.497
C3−N	1.347	1.244	1.320	1.331	1.335
N−C(CH_3)	1.468	1.500	1.463	1.470	1.475

dppm, dppe), which adds methanol across the $C_1{=}C_2$ double bond.[20a] If, however, two PPh_3 ligands are present instead, the nucleophile again adds to C_3. All this underlines that in rationalizing the regioselectivity of nucleophilic addition on the basis of theory, steric effects cannot be neglected and may even determine the regiochemistry.

(b) Aminoallenylidene Complexes 4. The orbital scheme of the model complex *trans*-$[Cl(PH_3)_4RuCCC(CH_3)N(CH_3)_2]^+$, representing our real aminoallenylidene complexes **4a**−**f**, is displayed on the right-hand side of Figure 8. As shown by the comparison in Table 8, the DFT-optimized geometry reproduces the key features of the experimental structures with reasonable accuracy. While most bond parameters agree within the standard deviations, larger differences are observed for the individual C−N bonds, which, however, suffer from some disorder of the NMe_2 unit and the butenyl side chain in the experimental structures.

Again, the crucial orbital interactions in the frontier orbitals involve the metal fragment and the unsaturated ligand. As shown in Table 9, the highest occupied levels are largely made up of the ruthenium and chlorine atoms (SHOMO, 80%; HOMO, 79%; SHOMO = second highest occupied molecular orbital) with only smaller contributions of the aminoallenylidene ligand (SHOMO, 13%; HOMO, 16%) mainly arising from C_2. The LUMO, in contrast, is delocalized over the unsaturated ligand (81%) with major contributions from C_1, C_3, and the $N(CH_3)_2$ substituent. The contributions of the metal and the chlorine are concomitantly small (10%). This pattern qualitatively agrees with that for the related all-carbon-substituted allenylidene complexes $[Cp(CO)(PH_3){=}C{=}C{=}CH_2]^+$ [20b] and $[CpL(PH)_3Os{=}C{=}C{=}CH_2]^{n+}$ (L = Cl, n = 0; L = PH_3, CO, n = 1)[20c] calculated at the EHT level, where the allenylidene ligand contributes about 25−30% to the HOMO and some 60−64% to the LUMO. Introducing an amino substituent at C_3 seemingly has a 2-fold effect in comparison to all-carbon-substituted analogues: the HOMO and the LUMO are even more localized on the metal and the allenylidene ligand, respectively. Second, as based on Mulliken analysis (see Table 7), the charge is distributed much more evenly over the aminoallenylidene ligand, as compared to related complexes of the parent allenylidene ligand, which indicates a somewhat smaller polarization of the unsaturated chain.

Table 9. ADF Calculated One-Electron Energies and Percentage Composition of Selected Highest Occupied and Lowest Unoccupied Molecular Orbitals of $[Cl(PH_3)_4RuC_3(CH_3)(N(CH_3)_2)]^+$ Expressed in Terms of Composing Fragments

MO	E (eV)	prevailing character	Ru	C_1	C_2	C_3	$N(CH_3)_2$	Cl
unocc								
33a′	−4.61	$Ru(Cl)(PH_3)_4$	32 (d)					12
32a′	−5.00	$Ru(Cl)(PH_3)_4$	41 (d)					
16a″	−5.90	π^* R′ + d_{Ru}	10 (d)	27	2	34	18	1
occ								
31a′	−7.85	Ru + Cl + π^* R′	35 (d)	1	14	1	0	44
15a″	−8.06	$Ru(Cl)(PH_3)_4$	23 (d)	0	6	2	5	57
30a′	−8.88	Ru + Cl + π^* R′	13	11	20	1	0	41
14a″	−9.06	Ru + Cl + π^* R′	17	6	19	1	14	28
13a″	−9.44	$Ru(Cl)(PH_3)_4$	74					

The close-lying occupied 15a″ and 31a′ and the lowest unoccupied 16a″ orbitals deserve some more comment, since they form the key to undestanding the optical properties of our aminoallenylidene complexes. Plots of these frontier orbitals are presented in Figure 10. In the SHOMO and the LUMO the π-system of the aminoallenylidene ligand is orthogonal to the $RuC_3(CH_3)(N(CH_3)_2)$ plane, while it is parallel for the HOMO. The HOMO/LUMO transition is thus symmetry-forbidden, while the SHOMO/LUMO transition is symmetry-allowed, as is experimentally observed. Following from the above discussion, both transitions have strong MLCT character. The two other features in our experimental spectra are assigned as follows. The less intense absorption at ca. 450 nm superimposed on the low-energy side of the SHOMO/LUMO absorption band is proposed to arise from the spin-forbidden singlet−triplet SHOMO/LUMO transition. The rather intense high-energy band at ca. 265−290 nm, often obscured by the PPh_2-based transitions but clearly visible as an isolated

(47) (a) Cadierno, V.; Gamasa, M. P.; Gimeno, J.; Lastra, E. *J. Organomet. Chem.* **1994**, *474*, C27. (b) Cadierno, V.; Gamasa, M. P.; Gimeno, J.; Borge, J.; García-Granda, S. *J. Chem. Soc., Chem. Commun.* **1994**, 2495. (c) Gamasa, M. P.; Gimeno, J.; González-Bernardo, C.; Borge, J.; García-Granda, S. *Organometallics* **1997**, *16*, 2483. (d) Cadierno, V.; Gamasa, M. P.; Borge, J. *Organometallics* **1997**, *16*, 3178. (e) Cadierno, V.; Gamasa, M. P.; Gimeno, J.; López-González, M. C.; Borge, J.; García-Granda, S. *Organometallics* **1997**, *16*, 4453. (f) Cadierno, V.; Gamasa, M. P.; Gimeno, J.; Pérez-Carreño, E.; Ienco, E. *Organometallics* **1998**, *17*, 5216.

(48) (a) Pirio, N.; Touchard, D.; Dixneuf, P. H. *J. Chem. Soc., Chem. Commun.* **1991**, 980. (b) Pirio, N.; Touchard, D.; Dixneuf, P. H. *J. Organomet. Chem.* **1993**, *462*, C18. (c) Touchard, D.; Pirio, N.; Dixneuf, P. H. *Organometallics* **1995**, *14*, 4920. (d) Esteruelas, M. E.; Gómez, A. V.; López, A. M.; Puerta, M. C.; Valerga, P. *Organometallics* **1998**, *17*, 4959. (e) Esteruelas, M. E.; Gómez, A. V.; López, A. M.; Modrego, J.; Oñate, E. *Organometallics* **1998**, *17*, 5434. (f) Bernard, D. J.; Esteruelas, M. E.; López, A. M.; Modrego, J.; Puerta, M. C.; Valerga, P. *Organometallics* **1999**, *18*, 4995.

(49) (a) Werner, H.; Wiedemann, R.; Laubender, M.; Wolf, J.; Windmüller, B. *J. Chem. Soc., Chem. Commun.* **1996**, 1413. (b) Werner, H.; Wiedemann, R.; Steinert, P.; Wolf, J. *Chem. Eur. J.* **1997**, *3*, 127. (c) Laubender, M.; Werner, H. *Angew. Chem.* **1998**, *110*, 158.

(50) Ouzzine, K.; Dixneuf, P. H. *J. Chem. Soc., Chem. Commun.* **1989**, 219. (b) Pilette, D.; Ouzzine, K.; Le Bozec, H.; Dixneuf, P. H.; Rickard, C. E. F.; Roper, W. E. *Organometallics* **1992**, *11*, 809. (c) Touchard, D.; Pirio, N.; Dixneuf, P. H. *Organometallics* **1995**, *14*, 4920.

(51) Bruce, M. I.; Low, P. J.; Tiekink, E. R. T. *J. Organomet. Chem.* **1999**, *572*, 3.

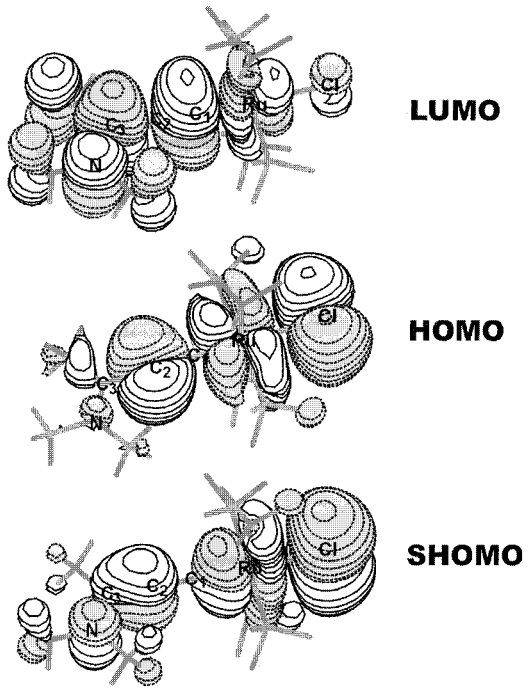

Figure 10. Graphic representations of the frontier orbitals of the aminoallenylidene model complex $[Cl(PH_3)_4RuC_3\{N(CH_3)_2\}(CH_3)]^+$.

band for the depe complex **4c**, results from an excitation into the LUMO from the lower lying 14a″ level. To further support our assignments, the energetically lowest transitions as well as their oscillator strengths were calculated by time-dependent (TD) DFT methods within the G98/B3LYP and the ADF/BP approximations. The results reasonably agree with our experimental data, as shown by the comparison in Table 10. Although the absolute values of transition energies and oscillator strengths clearly depend on the computational method employed, the data correctly reproduce the sequence of transitions and, at least qualitatively, the relative band intensities.

One last point concerns the assignment of the two prominent infrared bands in the 2000−1500 cm^{-1} region. Frequency calculations based on the G98/B3LYP method place the first band at 1998 cm^{-1}. This band is essentially the symmetric stretch of the C_1C_2 bond involving the carbon atom directly attached to the metal. The second feature is calculated to occur at 1524 cm^{-1}. It arises from the C═N stretch coupled with the bending of the three methyl groups surrounding the iminium moiety.

Consequences of Electron Transfer on the Bonding. One important question is how electron transfer from aminoallenylidene complexes **4** affects the bonding within these systems. Geometry optimization of the oxidized forms was performed in the $^2A'$ and $^2A''$ states, which differ in the ordering of the 16a″ and 32a′ levels. We note that the UV/vis spectra suggest that the level ordering 16a″ < 32a′ is maintained in the oxidized state. Our calculations indicate that most of the structural reorganization is confined to the ClP_4Ru fragment (see Table 8). The most important structural changes are the shortening of the Ru−Cl bond by about 0.1 Å and the lengthening of the Ru−P bonds by about 0.05 Å. This is easily understood on the basis of our DFT calculations and the Ru(II/III) character of the oxidation process. The highest lying occupied levels are both Ru−Cl antibonding in nature: hence, the Ru−Cl bond shortening. Upon oxidation, the metal center loses electron density, which leads to smaller back-donation to the π-acidic phosphine ligands, in accord with the lengthening of the Ru−P bonds. This is consistent with experimental evidence from the complexes $[MXY(L_2)_2]$ (X, Y = CN, Cl, L_2 = 2 PR_3, chelating diphosphine), which have been characterized crystallographically in both adjacent oxidation states.[52] In contrast, the metrical parameters of the aminoallenylidene ligand change to only a very minor degree with some lengthening of the C_2-C_3 and some shortening of the C_3-N bond. These structural changes taken per se are best interpreted in terms of an even higher weight of the iminium alkynyl type resonance form in the oxidized state, i.e., *trans*-$[Cl(dppm)_2Ru'-C{\equiv}CC(=NMe_2)CH_3]^{2+}$, consistent with a metal-based oxidation process.

With their characteristic and intense C≡C and C═N IR bands, aminoallenylidene complexes **4** appear especially well suited to monitor changes in the bonding sequence along the unsaturated ligand by spectroelectrochemistry. The direction of the band shift is of special relevance: For mononuclear alkynyl complexes a moderate shift of the C≡C stretch to *higher energies* usually accompanies oxidation, although some results to the contrary have also been reported.[33] In particular, the latter situation holds if the oxidation leads to a higher contribution of a cumulene type resonance form, as observed for ferrocenyl− or ruthenocenyl−acetylide complexes[52] or with C_4-bridged dimetal complexes.[2−5] Band shifts are considerably higher in this case, often exceeding 100 cm^{-1}. With reference to Table 4, it is difficult to reconcile our experimental data with the results from theory. In every case the CC band is displaced to considerably lower energy upon oxidation. With the exception of the piperidine-substituted complex **4d**, where the piperidine ring may act as a stronger donor in the oxidized state, the same also holds for the C═N stretch. Both observations rather agree with a higher cumulenic character in the Ru(III) state. On the other hand, we have observed an exactly opposite shift of ν_{CC} from 1997 to 2022 cm^{-1} for the second, ruthenium-based oxidation of the aminoallenylidene complex $[Cl(dppm)_2Ru-C{\equiv}CC(=NMe_2)C_2H_4Fc]^+$ with an appended redox-active ferrocenyl (Fc) moiety. At this point we cannot offer a conclusive explanation for this apparently controversial behavior. Another striking observation is the large decrease in absorptivity of the CC band upon oxidation to the Ru(III) dications. Our working hypothesis is as follows: in the oxidized state the C_1C_2 unit bridges *two positively charged centers* (the metal and the heteroatom), and this is expected to decrease the dipole moment change during the symmetric stretch as opposed to the monocationic Ru(II) state. Interestingly, and in good agreement with this view, the CC band is

(52) (a) Carvalho, M. F. N. N.; Duarte, M. T.; Galvão, A. M.; Pombeiro, A. J. L.; Henderson, R.; Fuess, H.; Svoboda, I. *J. Organomet. Chem.* **1999**, *583*, 56. (b) Salih, T. A.; Duarte, M. T.; Fraústo da Silva, J. J. R.; Galvão, A. M.; Guedes da Silva, M. F. C.; Hitchcock, P. B.; Hughes, D. L.; Pickett, C. J.; Pombeiro, A. J. L.; Richards, R. L. *J. Chem. Soc., Dalton Trans.* **1993**, 3015.

Table 10. Lowest Calculated TD DFT Excitation Energies (eV) for $[Cl(PH_3)_4RuC_3(CH_3)(N(CH_3)_2)]^+$

		G98/B3LYP		ADF/BP			
state	main components	transition energy (eV)	osc[a] str	transition energy (eV)	osc[a] str	exptl transition, **4c** (eV)	log ϵ
$^3A''$	99% (31a′ → 16a″)	2.29		1.91			
$^1A''$	99% (31a′ → 16a″)	2.43	0.000	1.98	0.0001	1.97	2.58
$^3A'$	98% (15a″ → 16a″)	2.48		2.04		2.52	2.55
$^1A'$	88% (15a“→ 16a″)	3.31	0.271	2.53	0.120	3.10	4.34
$^1A'$	98% (31a′→ 32a′)	3.51	0.007	2.96	0.001	no[b]	no
$^1A'$	77% (14a″ → 16a″), 8% (15a″ → 16a″)	4.106	0.201	3.85	0.285	4.32	3.06
$^1A'$	98% (30a′ → 32a′)			3.95	0.001		

[a] Oscillator strength. [b] no = not observed.

reported to also be much weaker in *neutral* allenylidene complexes than in *monocationic* ones.[54]

Conclusion

Aminoallenylidene complexes *trans*-$[Cl(L_2)_2RuCCC(NR_2)(CH_2R')]^+$ (**4**) are accessible by a one-pot procedure where the unsaturated C_7N ligand is assembled from butadiyne and an allylic or propargylic amine via primary butatrienylidene complexes *trans*-$[Cl(L_2)_2Ru{=}C{=}C{=}C{=}CH_2]^+$ as the reactive intermediates and amine adducts *trans*-$[Cl(L_2)_2Ru{-}C{\equiv}CC(NR_2R'){=}CH_2]^+$ formed by nucleophilic addition to the cumulated C_4 ligand. If R′ is an allylic moiety, the amine adducts rearrange under mild conditions via an Aza-Cope type process to their aminoallenylidene isomers, whereas in the propargylic case the barrier is higher such that the primary adduct is isolable and its rearrangement can be independently studied. Along the continuum between true cumulenic $[\{Ru\}{=}C{=}C{=}C(ER_n)R']^+$ and alkynyl type $[\{Ru\}{-}C{\equiv}CC(=ER_n)R']^+$ resonance descriptions,[13c] aminoallenylidene complexes so far display the highest alkynyl character of the whole series ER_n = NR_2, OR, SR, SeR, CR_3. Indications are the energy barriers for rotation around the C=N bond in NMR spectroscopy, the position of the $Ru{-}C_1C_2$ stretch and the intense C=N band at ca. 1550 cm^{-1} in their IR spectra, and the considerable bond length alternation along the RuC_3N entity with a short C3−N bond and planar coordination of the iminium nitrogen, as established by X-ray crystallography. The role of the metal center is evident from complexes **4a**−**c**, which only differ in their diphosphine chelate ligands. A more basic metal fragment enhances the cumulenic character of the allenylidene chain.

DFT calculations on a simplified model of our proposed butatrienylidene intermediate establish that combined orbital (i.e. the orbital coefficients at the LUMO) and steric (i.e. the shielding of C_1 by the bulky coligands on the metal) effects are responsible for the highly regioselective nucleophilic attack on C_3. Our results on the aminoallenylidene model complex *trans*-$[Cl(PH_3)_4RuCCC\{N(CH_3)_2\}(CH_3)]^+$ support the idea of a metal-based oxidation and a ligand-based reduction,[13c] which is fully consistent with our experimental results. These calculations also aid in the assignment of the main absorption bands in their electronic and IR spectra.

Experimental Section

All manipulations were performed by standard Schlenk techniques under an argon atmosphere. Dichloromethane, hexanes, and acetonitrile were dried by disitillation from CaH_2; xylene was dried over sodium. *o*-Dichlorobenzene was used without further purification. All solvents were degassed by either at least three freeze−pump−thaw cycles or saturation with argon prior to use. $RuCl_2(dmso)_4$[55] and *cis*-$RuCl_2(dppm)_2$[56] were obtained according to literature methods, while *trans*-$RuCl_2(dppe)_2$ was prepared as outlined below. Butadiyne was prepared from 1,4-dichloro-2-butyne as detailed in an earlier publication[13d] and isolated at 195 K as a white, crystalline solid. *Caution! Butadiyne should be handled and stored under rigorous exclusion of air and at temperatures below 230 K.* The respective amines were obtained from commercial sources or prepared from their hydrochlorides by standard procedures and distilled from KOH before use. Yields given for complexes **3f**,**g** and **4a**−**f** are based on *cis*-$RuCl_2(dppm)_2$. Infrared spectra were obtained on a Perkin-Elmer Paragon 1000 PC FT-IR instrument. ^1H (250.13 MHz), ^{13}C (62.90 MHz), and ^{31}P NMR spectra (101.26 MHz) were recorded on a Bruker AC 250 spectrometer at 303 K in the solvent indicated. The spectra were referenced to residual protonated solvent (^1H), the solvent signal itself (^{13}C), or external H_3PO_4 (^{31}P). The assignment of ^{13}C NMR spectra was aided by DEPT-135 experiments. UV/vis spectra were obtained on a Shimadzu UV-160 spectrometer or an Omega 10 spectrometer from Bruins Instruments. The EPR equipment consists of a Bruker ESP 3000 spectrometer equipped with an HP frequency counter 5350 B, a Bruker NMR gaussmeter ER 035 M, and a continuous flow cryostat ESR 900 from Oxford Instruments for low-temperature work. Elemental analyses (C, H, N) were performed at in-house facilities. All electrochemical experiments were performed in a home-built cylindrical vacuumtight one-compartment cell. A spiral-shaped Pt wire and an Ag wire as the counter and reference electrodes are sealed directly into opposite sides of the glass wall while the respective working electrode (Pt or glassy carbon 1.1 mm polished with 0.25 μm diamond paste (Buehler-Wirtz) before each experiment) is introduced via a Teflon screw cap with a suitable fitting. The cell may be attached to a conventional Schlenk line via two side arms equipped with Teflon screw valves and allows experiments to be performed under an atmosphere of argon with approximately 2.5 mL of analyte solution. Solvents for electrochemistry were obtained in the highest available purity from commercial sources (CH_2Cl_2 and 1,2-$C_2H_4Cl_2$ from Fluka (Burdick&Jackson brand), CH_3CN (HPLC gradient grade) from Roth, THF (99.9%) from Aldrich) and freshly distilled from CaH_2 (CH_2Cl_2, 1,2-$C_2H_4Cl_2$, CH_3CN) or K (THF) before use. NBu_4PF_6 (0.25 mM) was used as the supporting electrolyte. All potentials are reported relative to the internal ferrocene/ferrocenium couple. Electrochemical data were ac-

(53) (a) Sato, M.; Hayashi, Y.; Kumakura, S.; Shimizu, N.; Katada, M.; Kawata, S. *Organometallics* **1996**, *15*, 761. (b) Sato, M.; Kawata, Y.; Shintate, H.; Habata, Y.; Akabori, S.; Unoura, K. *Organometallics* **1997**, *16*, 1693. (c) Sato, M.; Iwai, A.; Watanabe, M. *Organometallics* **1999**, *18*, 3208.

(54) Harlow, K. J.; Hill, A. F.; Wilton-Ely, J. D. E. T. *J. Chem. Soc., Dalton Trans.* **1999**, 285.

(55) Evans, I. P.; Spencer, A.; Wilkinson, G. *J. Chem. Soc., Dalton Trans.* **1973**, 204.

(56) Chaudret, B.; Commenges, G.; Poilblanc, R. *J. Chem. Soc., Dalton Trans.* **1984**, 1635.

quired with a computer-controlled EG&G Model 273 potentiostat utilizing the EG&G 250 software package. The OTTLE cell was also home-built and comprises a Pt-mesh working and counter electrode and a thin silver wire as a pseudo-reference electrode sandwiched between the CaF_2 windows of a conventional liquid IR cell. The working electrode is positioned in the center of the spectrometer beam.

Calculations. Ground-state electronic structure calculations on $[Cl(PH_3)_4RuC_3\{N(CH_3)_2\}CH_3]^+$ and $[ClRu(PH_3)_4C_4H_2]^+$ have been performed by density functional theory (DFT) methods using the Amsterdam density functional (ADF1999)[57,58] and Gaussian 98[59] program packages. The lowest excited states of the closed-shell complexes were calculated by the time-dependent DFT method (ADF-RESPONSE[60] program and Gaussian 98). Within Gaussian 98 Dunning's valence double-ξ functions[60] with polarization functions were used for C, N, and H atoms and the effective quasirelativistic effective core pseudopotentials and corresponding optimized set of basis functions for P,[61] Cl,[61] and Ru[62] atoms. A hybrid Becke three-parameter functional with Lee, Yang, and Parr correlation functional (B3LYP)[63] was used in Gaussian 98 calculations (G98/B3LYP). Within the ADF program Slater type orbital (STO) basis sets of double-ξ quality with polarization functions for H, C, N, P, and Cl atoms and triple-ξ functions for Ru were employed. Inner shells were treated within the frozen-core approximation (1s for C and N, 1s−2p for P and Cl, 1s−3d for Ru). Local density approximation (LDA) with VWN parametrization of electron gas data, including Becke's gradient correction[64] to the local exchange expression in conjunction with Perdew's gradient correction[65] to the LDA correlation, was used (ADF/BP). The scalar relativistic (SR) zero-order regular approximation (ZORA) was used within this study. The adiabatic local density approximation (ALDA), with the frequency dependence ignored, was used in post-SCF time-dependent DFT calculations (TD-DFT). The calculated IR frequencies were scaled as recommended for DFT calculations with the double-ξ basis set.[66] Due to their size the real complexes were approximated by model systems where P-containing ligands were replaced by PH_3 groups. The symmetry was constrained to C_s or C_{2v} point groups throughout the calculations.

***trans*-$RuCl_2(dppe)_2$.** $RuCl_2(dmso)_4$ (0.848 g, 1.75 mmol) and 1,2-bis(diphenylphosphino)ethane (dppe, 1.44 g, 3.5 mmol) were suspended in xylene (70 mL) and put under reflux. Within few minutes a clear yellow solution was obtained which gradually darkened to orange-yellow with the concomitant formation of some dark yellow precipitate. After 7 h the suspension was cooled to room temperature and then stored at +4 °C overnight. The dark yellow solid was collected by filtration, washed with three 15 mL portions of ether and hexanes each, and then dried in vacuo. A second crop was obtained after concentrating the mother liquor to about 8 mL and precipitating with ether. Combined yield: 1.485 g, 87.6%.

***trans*-$[Cl(dppm)_2RuC_3(NMe_2)C_2H_4CH{=}CH_2]^+$ (4a).** To a mixture of solid *cis*-$RuCl_2(dppm)_2$ (0.136 g, 0.145 mmol) and $NaPF_6$ (0.097 g, 0.578 mmol) was added excess butadiyne dissolved in CH_2Cl_2 (30 mL). After approximately 30 min the reaction mixture turned green. At this point $NMe_2C_3H_5$ (100 μL, 0.85 mmol) was added by syringe. The solution was stirred under ambient conditions under occasional IR control. When the intensity of the allenylidene band near 1900 cm^{-1} remained unchanged (ca. 22 h), excess $NaPF_6$ and the NaCl formed were removed by cannula filtration and the solvent was driven off under reduced pressure. Purification was achieved by column chromatography on basic alumina (eluant CH_2Cl_2/CH_3CN 12:1). The first, intensely yellow-green fraction was collected. The oily residue that remained after evaporation of solvents was triturated with ether, and the resulting green powder was dried in vacuo to give 0.087 g (0.073 mmol, 51%) of **4a**. ^1H NMR ($CDCl_3$): δ 1.35 (m, CH_2 (butenyl), 2H), 1.52 (m, CH_2 (butenyl), 2H), 2.02 (s, NCH_3, 3H), 2.82 (s, NCH_3, 3H), 4.77 (dd, trans HC=C*H*H, $^2J_{H-H}$ = 1.4 Hz, $^3J_{H-H}$ = 17.0 Hz, 1H), 4.77 (m, CH_2 (dppm), 2H), 4.92 (dd, *cis*-HC=C*H*H, $^2J_{H-H}$ = 1.4 Hz, $^3J_{H-H}$ = 10.2 Hz, 1H), 5.09 (dquint, CH_2 (dppm), J_{H-H} = 14.9 Hz, $^2J_{P-H}$ = $^3J_{P-H}$ = 4.4 Hz, 2H), 5.34 (m, *H*C=CH_2, 1H), 7.13 (m, aryl H (dppm), 8H), 7.23 (m, aryl H (dppm), 20H), 7.41 (m, aryl H (dppm), 4H), 7.53 (m, aryl H (dppm), 8H). $^{13}C\{^1H\}$ NMR ($CDCl_3$): δ 28.9 (CH_2 (butenyl)), 35.5 (CH_2 (butenyl)), 40.4 (CH_3N), 43.2 (CH_3N), 48.7 (vquint, CH_2 (dppm), N_{P-C} = 11.1 Hz), 116.2 (C=*C*H_2 (butenyl)), 118.7 (C2), 127.9 (m, *m*-C_6H_5, N_{P-C} = 2.3 Hz), 128.5 (m, *m*-C_6H_5, N_{P-C} = 2.2 Hz), 130.0, 130.7 (*p*-C_6H_5), 132.5 (vquint, *ipso*-C_6H_5, N_{P-C} = 11.7 Hz), 133.0 (m, *o*-C_6H_5, N_{P-C} = 2.9 Hz), 133.4 (m, *o*-C_6H_5, N_{P-C} = 2.8 Hz), 134.1 (vquint, *ipso*-C_6H_5, N_{P-C} = 11.2 Hz), 135.2 (*C*=CH_2 (butenyl)), 156.9 (C3), 202.1 (quint, C1, J_{P-C} = 13.9 Hz); $^{31}P\{^1H\}$ NMR ($CDCl_3$, H_3PO_4 (ext)): δ −8.2 (s, P (dppm)), −143.6 (sept, PF_6^-, J_{P-F} = 708 Hz). IR (KBr; cm^{-1}): ν(CC) 1995 (s), ν(C=N) 1572 (m). UV/vis (CH_3CN; λ_{max}, nm (log ϵ)): 209 (4.94), 229 (4.86), 264 (sh), 384 (4.13), 465 (sh, 2.89), 635 (2.48). Anal. Calcd for $C_{59}H_{57}ClF_6NP_5Ru$: C,59.78; H, 4.84; N, 1.18. Found: C, 59.05; H, 4.82; N, 1.21.

***trans*-$[Cl(dppe)_2RuC_3(NMe_2)C_2H_4CH{=}CH_2]^+SbF_6^-$ (4b).** *trans*-$RuCl_2(dppe)_2$ (0.248 g, 0.256 mmol) and $NaSbF_6$ (0.290 g, 1.12 mmol) were suspended in *o*-$C_6H_4Cl_2$, and excess butadiyne (ca. 700 μL) was added. The suspension was stirred for 45 min at room temperature, and $NMe_2C_3H_5$ (90 μL, 0.76 mmol) was added by syringe. After 3 days a clear orange solution with some white precipitate (excess $NaSbF_6$ and NaCl) had formed, which exhibited an intense IR absorption band at 1983 cm^{-1}. After filtration the solvent was driven off in vacuo and the oily residue was repeatedly washed with 5 mL portions of hexanes. The orange-red powdery residue was then recrystallized from CH_2Cl_2/hexane to yield orange-red crystals of **4b**·$3CH_2Cl_2$. Two more batches were obtained upon further concentration of the mother liquors to give a total yield of 0.335 g (83.9%). ^1H NMR (CD_2Cl_2): δ 1.27 (m, CH_2 (butenyl), 2H), 1.46 (m, CH_2 (butenyl), 2H), 2.62 (br, CH_2 (dppe), 4H), 2.78 (s, NCH_3, 3H), 2.92 (br, CH_2 (dppe), 4H), 3.30 (s, NCH_3, 3H), 5.05 (dd, trans HC=C*H*H, $^2J_{H-H}$ = 1.1 Hz, $^3J_{H-H}$ = 17.2 Hz, 1H), 5.11 (dd, *cis*-HC=C*H*H, $^2J_{H-H}$ = 1.1 Hz, $^3J_{H-H}$ = 10.3 Hz, 1H),

(57) Baerends, E. J.; Bérces, A.; Bo, C.; Boerrigter, P. M.; Cavallo, L.; Deng, L.; Dickson, R. M.; Ellis, D. E.; Fan, L.; Fischer, T. H.; Fonseca Guerra, C.; van Gisbergen, S. J. A.; Groeneveld, J. A.; Gritsenko, O. V.; Harris, F. E.; van den Hoek, P.; Jacobsen, H.; van Kessel, G.; Kootstra, F.; van Lenthe, E.; Osinga, P. V.; Philipsen, P. H. T.; Post, D.; Pye, C. C.; Ravenek, W.; Ros, P.; Schipper, P. R. T.; Schreckenbach, G.; Snijders, J. G.; Sola, M.; Swerhone, D.; te Velde, G.; Vernooijs, P.; Versluis, L.; Visser, O.; van Wezenbeek, E.; Wiesenekker, G.; Wolff, S. K.; Woo, T. K.; Ziegler, T. *ADF 1999.01*; Amsterdam, 1999.

(58) Fonseca Guerra, C.; Snijders, J. G.; te Velde, G.; Baerends, E. J. *Theor. Chem. Acc.* **1998**, *99*, 391.

(59) Frisch, M. J.; Trucks, G. W.; Schlegel, H. B.; Scuseria, G. E.; Robb, M. A.; Cheeseman, J. R.; Zakrzewski, V. G.; Montgomery, J. A., Jr.; Stratmann, R. E.; Burant, J. C.; Dapprich, S.; Millam, J. M.; Daniels, A. D.; Kudin, K. N.; Strain, M. C.; Farkas, O.; Tomasi, J.; Barone, V.; Cossi, M.; Cammi, R.; Mennucci, B.; Pomelli, C.; Adamo, C.; Clifford, S.; Ochterski, J.; Petersson, G. A.; Ayala, P. Y.; Cui, Q.; Morokuma, K.; Malick, D. K.; Rabuck, A. D.; Raghavachari, K.; Foresman, J. B.; Cioslowski, J.; Ortiz, J. V.; Stefanov, B. B.; Liu, G.; Liashenko, A.; Piskorz, P.; Komaromi, I.; Gomperts, R.; Martin, R. L.; Fox, D. J.; Keith, T.; Al-Laham, M. A.; Peng, C. Y.; Nanayakkara, A.; Gonzalez, C.; Challacombe, M.; Gill, P. M. W.; Johnson, B.; Chen, W.; Wong, M. W.; Andres, J. L.; Gonzalez, C.; Head-Gordon, M.; Replogle, E. S.; Pople, J. A. *Gaussian 98*, Revision A.7; Gaussian, Inc.: Pittsburgh, PA, 1998.

(60) Woon, D. E.; Dunning, T. H., Jr. *J. Chem. Phys.* **1993**, *98*, 1358.

(61) Bergner, A.; Dolg, M.; Kuechle, W.; Stoll, H.; Preuss, H. *Mol. Phys.* **1993**, *80*, 1431.

(62) Andrae, D.; Haeussermann, U.; Dolg, M.; Stoll, H.; Preuss, H. *Theor. Chim. Acta* **1990**, *77*, 123.

(63) Stephens, P. J.; Devlin, F. J.; Cabalowski, C. F.; Frisch, M. J. *J. Phys. Chem.* **1994**, *98*, 11623.

(64) Becke, A. D. *Phys. Rev. A* **1988**, *38*, 3098.

(65) Perdew, J. P. *Phys. Rev. A* **1986**, *33*, 8822.

(66) Wong, M. W. *Chem. Phys. Lett.* **1996**, *256*, 391.

(67) Sheldrick, G. M. SHELX-97: Program for Crystal Structure Determination from Diffraction Data; University of Göttingen: Göttingen, Germany, 1997.

5.33 (CH_2Cl_2), 5.72 (ddd, HC═CH_2, 1H, $^2J_{H-H}$ = 1.1 Hz, $^3J_{H-H}$ = 10.3, 6.2 Hz), 6.63 (m, aryl H (dppm), 8H), 7.15 (t, aryl H (dppm), $^3J_{H-H}$ = 7.6 Hz, 8H), 7.30 (t, aryl H (dppm), $^3J_{H-H}$ = 7.6 Hz, 8H), 7.41 (t, aryl H (dppm), $^3J_{H-H}$ = 7.3 Hz, 4H), 7.51 (t, aryl H (dppm), $^3J_{H-H}$ = 7.3 Hz, 4H), 7.65 (br, aryl H (dppm), 8H). $^{13}C\{^1H\}$ NMR ($CDCl_3$): δ 30.2 (CH_2 (butenyl)), 30.3 (quint, CH_2 (dppe), J_{P-C} = 7.0 Hz), 36.4 (CH_2 (butenyl)), 42.1 (CH_3N), 44.8 (CH_3N), 117.6 (C═CH_2 (butenyl)), 118.8 (quint, C2, J_{P-C} = 1.6 Hz), 129.1 (quint, *m*-C_6H_5, N_{P-C} = 2.4 Hz), 129.3 (quint, *m*-C_6H_5, N_{P-C} = 2.1 Hz), 131.2, 132.2 (*p*-C_6H_5), 131.6 (quint, *ipso*-C_6H_5, N_{P-C} = 10.6 Hz), 132.5 (quint, *o*-C_6H_5, N_{P-C} = 2.2 Hz), 132.8 (quint, *ipso*-C_6H_5, N_{P-C} = 11.5 Hz), 134.3 (quint, N_{P-C} = 2.8 Hz, *o*-C_6H_5), 134.7 (*C*═CH_2 (butenyl)), 160.2 (quint, C3, J_{P-C} = 1.2 Hz), 189.5 (quint, C1, J_{P-C} = 14.5 Hz). $^{31}P\{^1H\}$ NMR ($CDCl_3$): δ 46.6 (s, P (dppe)). IR (KBr; cm^{-1}): ν(CC) 2005 (s), ν(C═N) 1585 (m). UV/vis (CH_3CN; λ_{max}, nm (log ϵ)): 203 (4.87), 223 (sh, 4.70), 253 (4.61), 268 (sh, 4.43), 325 (sh, 3.78), 364 (4.12), 415 (sh, 3.32), 688 (1.90). Anal. Calcd for $C_{61}H_{61}ClF_6NP_4RuSb{\cdot}3CH_2Cl_2$: C, 49.30; H, 4.33; N, 0.90. Found: C, 48.93; H, 4,34; N, 1.05.

***trans*-[Cl(depe)$_2$RuC$_3$(NMe$_2$)C$_2$H$_4$CH═CH$_2$]$^+$PF$_6^-$ (4c).** The synthesis was performed in analogy to compound **4a**, but starting from *cis*-$RuCl_2$(depe)$_2$ (0.156 g, 0.267 mmol), $NaPF_6$ (0.178 g, 1.06 mmol), butadiyne, and NMe_2allyl (190 μL, 1.61 mmol); CH_2Cl_2/CH_3CN (8:1) was used as the eluant in the chromatographic workup. After removal of the solvent a dark green oil was obtained which solidified after trituration with Et_2O. Yield: 0.078 g, 0.094 mmol, 35%. ^1H NMR ($CDCl_3$): δ 1.12 (m, CH_3(depe), 24H), 1.80 (m, CH_2 (depe), 16H), 2.05 (vsext, CH_2 (depe), $^3J_{P-H}$ = $^3J_{C-H}$ = $^2J_{C-H}$ = 7.4 Hz, 4H), 2.28 (m, CH_2 (butenyl), 2H), 2.31 (vsext, CH_2 (depe), $^3J_{P-H}$ = $^3J_{C-H}$ = $^2J_{C-H}$ = 7.6 Hz, 4H), 2.51 (m, CH_2 (butenyl), 2H), 3.18 (s, NCH_3, 3H), 3.28 (s, NCH_3, 3H), 5.01 (dd, *trans*-HC═CHH, $^2J_{H-H}$ = 1.3 Hz, $^3J_{H-H}$ = 18.9 Hz, 1H), 5.02 (dd, *cis*-HC═CHH, $^2J_{H-H}$ = 1.3 Hz, $^3J_{H-H}$ = 12.5 Hz, 1H), 5.27 (s, CH_2Cl_2), 5.75 (m, HC═CH_2 (butenyl), 1H). $^{13}C\{^1H\}$ NMR ($CDCl_3$): δ 9.0, 9.1 (CH_3(depe)), 17.10 (m, (CH_2 (depe), N_{P-C} = 6.3 Hz)), 19.8 (m, (CH_2 (depe), N_{P-C} = 6.6 Hz)), 20.4 (m, PCH_2CH_2P, N_{P-C} = 11.7 Hz), 30.9 (CH_2 (butenyl)), 37.4 (CH_2 (butenyl)), 40.7 (NCH_3), 44.4 (NCH_3), 116.5 (HC═CH_2), 117.9 (C2), 135.3 (H*C*═CH_2), 155.4 (C3), 211.1 (quint, C1, J_{P-C} = 13.7 Hz). $^{31}P\{^1H\}$ NMR ($CDCl_3$): δ 47.58 (s, P (depe)), −144.0 (sept, PF_6^- J_{P-F} = 707 Hz). IR (KBr; cm^{-1}): ν(CC) 1979 (vs), ν(C═N) 1564 (s). UV/vis (CH_3CN; λ_{max}, nm (log ϵ)): 215 (4.27), 287 (3.06), 400 (4.24), 491 (sh, 2.55), 626 (2.58). Anal. Calcd for $C_{29}H_{61}ClF_6NP_5Ru{\cdot}0.5CH_2Cl_2$: C, 40.65; H, 7.17; N, 1.61. Found: C, 40.84; H, 6,94; N, 1.59.

***trans*-[Cl(dppm)$_2$RuC$_3$(NC$_5$H$_{10}$)C$_2$H$_4$CH═CH$_2$]$^+$SbF$_6^-$ (4d).** This compound was prepared as described for **4a**. With 0.175 g (0.186 mmol) of *cis*-$RuCl_2$(dppm)$_2$, 0.186 g of $NaSbF_6$ (0.72 mmol), and 112 mg of allylpiperidine (0.89 mmol) as the starting materials, 0.152 g (0.116 mmol, 62.4%) of **4d** was obtained as a yellow-green powder after chromatographic workup on silica gel (CH_2Cl_2/CH_3CN (10:1) v/v) as eluant). ^1H NMR (CD_3CN): δ 1.0 (quint (br), CH_2 (pip), 2H, J_{H-H} = 4.9 Hz), 1.43−1.52 (m, CH_2 (pip) and CH_2 (butenyl), 8H), 2.70 (dd, NCH_2, 2H, J_{H-H} = 6.3, 5.9 Hz), 3.21 (m, br NCH_2, 2H), 4.85 (dquint, CH_2 (dppm), J_{H-H} = 15.1 Hz, $^2J_{P-H}$ = $^3J_{P-H}$ = 4.3 Hz, 2H), 4.86 (ddt, trans HC═C*H*H, $^2J_{H-H}$ = 1.7 Hz, $^3J_{H-H}$ = 16.9 Hz, $^4J_{H-H}$ = 0.8 Hz, 1H), 4.96 (ddd, *cis*-HC═C*H*H, $^2J_{H-H}$ = 1.7 Hz, $^3J_{H-H}$ = 10.2 Hz, $^4J_{H-H}$ = 0.8 Hz, 1H), 5.22 (dquint, CH_2 (dppm), J_{H-H} = 15.1 Hz, $^2J_{P-H}$ = $^3J_{P-H}$ = 4.6 Hz, 2H), 5.39 (m, H*C*═CH_2, 1H), 7.21 (m, aryl H (dppm), 8H), 7.31−7.47 (m, aryl H (dppm), 24H), 7.57 (m, aryl H (dppm), 8H). $^{13}C\{^1H\}$ NMR (CD_3CN): δ 23.6, 27.2, 27.4 (CH_2 (pip), 31.5, 36.4 (CH_2 (butenyl)), 48.9 (quint, CH_2 (dppm), N_{P-C} = 11.84 Hz), 50.7, 51.7 (CH_2N (pip), 116.8 (C═CH_2 (butenyl)), 119.4 (quint, C2, J_{P-C} = 1.57 Hz), 128.9, 129.5 (quint, *m*-C_6H_5, N_{P-C} = 2.6 Hz), 131.1, 131.6 (s, *p*-C_6H_5), 133.9 (quint, *o*-C_6H_5, N_{P-C} = 3.1 Hz), 134.1 (quint, *o*-C_6H_5, N_{P-C} = 3.2 Hz), 135.6 (quint, *ipso*-C_6H_5, N_{P-C} = 11.3 Hz), 136.6 (CH═CH_2 (butenyl)), 156.2 (quint, C3, J_{P-C} = 1.1 Hz), 202.2 (quint, C1, J_{P-C} = 13.9 Hz). $^{31}P\{^1H\}$ NMR ($CDCl_3$, H_3PO_4 (ext)): δ −8.1 (s, P (dppm)). IR (KBr; cm^{-1}): ν(CC) 1995 (vs), ν(C═N) 1553 (s). UV/vis (CH_3CN; λ_{max}, nm (log ϵ)): 211 (4.86), 227 (sh), 4.81), 266 (4.62), 391 (4.26), 435 (sh, 3.18), 654 (2.15). Anal. Calcd for $C_{62}H_{61}ClF_6NP_4RuSb$: C, 56.57; H, 4.67; N, 1.06. Found: C, 57.04; H, 4.62; N, 1.07.

***trans*-[Cl(dppm)$_2$RuC$_3$(NMe$_2$)CH$_2$CH(CH$_2$NMe$_2$)(CH═CH$_2$)]$^+$SbF$_6^-$ (4e).** *cis*-$RuCl_2$(dppm)$_2$ (0.181 g, 0.191 mmol) and $NaSbF_6$ (0.199 g, 0.77 mmol) were suspended in *o*-dichlorobenzene, and excess HC_4H was added. After the mixture was stirred for 45 min, the solution color had changed to apple green. At this point 0.681 g (85 μL, 0.48 mmol) of 1,4-bis(dimethylamino)but-2-ene was added by syringe. The reaction was stopped after the initial IR band at 2024 cm^{-1} of the simple adduct had totally disappeared and the much more intense absorption of the C_3 unit of the rearranged product at 1991 cm^{-1} remained unchanged (2 days). After filtration, the solvent was distilled off in vacuo. The tarry residue was vigorously stirred with ether (3 × 15 mL) and hexanes (2 × 10 mL) and then dried in vacuo to give the pure product as an orange yellow powder. Yield: 0.234 g, 92%. ^1H NMR (CD_2Cl_2): δ 1.27 (dd (br), $^2J_{H-H}$ = 21.1, $^3J_{H-H}$ = 12.3 Hz, 1H), 1.95 (m, CH_2, 4H), 2.09 (s, 3H, NMe), 2.17 (s, 6H, NMe_2), 2.94 (s, NMe, 3H), 3.21 (m, CH, 1H), 4.76 (dd, trans HC═C*H*H, $^2J_{H-H}$ = 2.1 Hz, $^3J_{H-H}$ = 16.5 Hz, 1H), 4.86 (dquint, CH_2 (dppm), J_{H-H} = 14.9 Hz, $^2J_{P-H}$ = $^3J_{P-H}$ = 4.4 Hz, 2H), 4.94 (dd, *cis*-HC═C*H*H, $^2J_{H-H}$ = 2.1 Hz, $^3J_{H-H}$ = 10.2 Hz, 1H), 5.04 (m, *H*C═CH_2, 1H), 5.23 (dquint, CH_2 (dppm), J_{H-H} = 14.9 Hz, $^2J_{P-H}$ = $^3J_{P-H}$ = 4.6 Hz, 2H) 7.23 (m, 7.21 (t, aryl H (dppm), $^3J_{H-H}$ = 7.3 Hz, 8H), 7.39 (m, aryl H (dppm), 18H), 7.50 (m, aryl H (dppm), 6H), 7.63 (m, aryl H (dppm), 8H). $^{13}C\{^1H\}$ NMR (CD_2Cl_2): δ 39.8 (CH_2), 40.6 (CH), 40.8, 43.3 (NCH_3), 45.7 ($N(CH_3)_2$), 48.1 (quint, CH_2 (dppm), N_{P-C} = 11.2 Hz), 63.5 (CH_2N), 116.7 (C═CH_2-(butenyl)), 120.8 (t, C2, J_{P-C} = 1.1 Hz), 127.9 (t, *m*-C_6H_5, J_{P-C} = 4.7 Hz), 128.0 (t, *m*-C_6H_5, J_{P-C} = 5.3 Hz), 128.6 (t, *m*-C_6H_5, J_{P-C} = 4.2 Hz), 128.71 (t, *m*-C_6H_5, J_{P-C} = 4.7 Hz), 130.1, 130.3, 130.7, 130.9 (*p*-C_6H_5), 132.4 (m, *ipso*-C_6H_5), 132.8, 133.1 (t, *o*-C_6H_5, J_{P-C} = 5.5 Hz), 133.3 (t, *o*-C_6H_5, J_{P-C} = 6.3 Hz), 133.5 (t, *o*-C_6H_5, J_{P-C} = 5.8 Hz), 134.2, 134.8 (m, *ipso*-C_6H_5, J_{P-C} = 11.3 Hz), 137.2 (*C*H═CH_2 (butenyl)), 156.7 (br, C3), 202.3 (quint, C1, J_{P-C} = 15.5 Hz). $^{31}P\{^1H\}$ NMR (CD_2Cl_2): δ −7.8 (AA′BB′ spin system, P (dppm)). IR (KBr; cm^{-1}): ν(CC) 1985 (vs), ν(C═N) 1582 (m). UV/vis (CH_3CN; λ_{max}, nm (log ϵ)): 217 (4.74), 228 (sh, 4.73), 265 (4.58), 325 (sh, 3.69), 388 (4.19), 465 (sh, 3.05). Anal. Calcd for $C_{62}H_{64}ClF_6N_2P_4RuSb$: C, 55.85; H, 4.84; N, 2.10. Found: C, 55.25; H, 4.68; N, 2.14.

***trans*-[ClRu(dppm)$_2$C≡CC(NMe$_2$CH$_2$C≡CEt)═CH$_2$]$^+$PF$_6^-$ (3f).** Solid *cis*-$RuCl_2$(dppm)$_2$ (0.220 g, 0.234 mmol) and $NaSbF_6$ (0.242 g, 0.93 mmol) were suspended in a solution of excess butadiyne in CH_2Cl_2 (30 mL). Within the next 40 min a color change from yellow to intense green was observed. The suspension was then cooled to +4 °C, and 1-(dimethylamino)pent-2-yne (250 μL, 0.202 g, 1.81 mmol) was added. The solution was stirred for 4 days at this temperature with occasional IR monitoring. Then it was filtered via a paper-tipped cannula and the solvent removed in vacuo. The oily residue was triturated with ether (2 × 15 mL), and the residual powdery solid was dried in vacuo. This crude product was then chromatographed on a silica column maintained at −3 °C. CH_2Cl_2/CH_3CN (25:2 v/v) eluted a bluish green band, which was collected. (A second olive green fraction provided a complex mixture of several compounds and was discarded.) The solvents were driven off in vacuo, and the remaining solid was washed with small portions of ether and dried to give 0.082 g (27%) of pure **3f**. ^1H NMR ($CDCl_3$): δ 1.12 (t, CH_2CH_3, $^3J_{H-H}$ = 7.5 Hz, 3H), 2.22 (qt, CH_2CH_3, $^3J_{H-H}$ = 7.5 Hz, $^5J_{H-H}$ = 2.2 Hz, 2H), 2.28 (s, 6H, NMe_2), 2.78 (t, CH_2N, $^5J_{H-H}$ = 2.2 Hz, 2H), 3.92 (d, C═C*H*H, $^2J_{H-H}$ = 3.1 Hz, 1H), 4.74 (d, C═CH*H*, $^2J_{H-H}$ = 3.1 Hz, 1H), 4.73 (dquint, CH_2 (dppm), J_{H-H} = 14.5 Hz, $^2J_{P-H}$ = $^4J_{P'-H}$ = 4.6 Hz, 2H), 4.96 (dquint, CH_2 (dppm),

J_{H-H} = 14.5 Hz, $^2J_{P-H}$ = $^4J_{P'-H}$ = 4.7 Hz, 2H), 7.09 (t, aryl H (dppm), $^3J_{H-H}$ = 7.4 Hz, 8H), 7.21 (t, aryl H (dppm), $^3J_{H-H}$ = 7.4 Hz, 10H), 7.27−7.33 (m, aryl H (dppm), 14H), 7.39 (m, aryl H (dppm), 8H). $^{13}C\{^1H\}$ NMR ($CDCl_3$): δ 12.5 (CH_2CH_3), 13.3 (CH_2CH_3), 49.5 ($N(CH_3)_2$), 49.8 (quint, CH_2 (dppm), N_{P-C} = 10.8 Hz), 54.7 (C3), 67.79 (NCH_2), 67.9, 94.3 (C≡C), 98.5 (br, C2), 106.8 (C=CH_2), 127.7, 128.4 (quint, *m*-C_6H_5, N_{P-C} = 2.2 Hz), 129.8, 130.1 (*p*-C_6H_5), 133.8 (quint, *o*-C_6H_5, N_{P-C} = 3.0 Hz), 132.9 (quint, *ipso*-C_6H_5, N_{P-C} = 11.2 Hz), 133.6 (quint, *o*-C_6H_5, N_{P-C} = 2.8 Hz), 135.28 (quint, *ipso*-C_6H_5, N_{P-C} = 11.1 Hz), 148.5 (quint, C1, J_{P-C} = 13.2 Hz). $^{31}P\{^1H\}$ NMR (101.3 MHz): δ −5.8 (s, P (dppm)). IR (KBr; cm^{-1}): ν(C≡C) 2033 (m), ν(C=C=C) 1996 (m), 1922 (w), ν(C=C) 1603 (w). UV/vis (CH_2Cl_2; λ_{max}, nm (log ϵ)): 266 (4.54), 319 (3.89), 640 (3.12). Anal. Calcd for $C_{61}H_{59}ClF_6NP_4RuSb$: C, 56.26; H, 4.57; N, 1.08. Found: C, 55.89; H, 4.52; N, 1.07.

***trans*-[Cl(dppm)$_2$RuC$_3$(NMe$_2$)CH$_2$C(C$_2$H$_5$)=C=CH$_2$]$^+$SbF$_6^-$ (4f).** Solid *cis*-$RuCl_2$(dppm)$_2$ (0.250 g, 0.266 mmol) and $NaSbF_6$ (0.258 g, 1.0 mmol) were suspended in *o*-dichlorobenzene (50 mL) to which excess butadiyne had been added. After the suspension had taken on a green coloration, 110 μL (0.089 g, 0.80 mmol) of 1-(dimethylamino)-2-pentyne was added by syringe. After 23 h of stirring under ambient conditions the pale green solution showed an IR band at 2032 cm^{-1} indicative of the formation of the primary adduct **3f**. The reaction vessel was immersed in an oil bath maintained at 65 °C, and the progress of the rearrangement was monitored by IR. This process was accompanied by a color change to intense yellow-green and the formation of a much more intense absorption at 1996 cm^{-1} at the expense of the 2032 cm^{-1} band. After 23 h excess $NaSbF_6$ and NaCl were filtered off and the solvent was removed by vacuum distillation. The slightly tarry residue was vigorously stirred with 10 mL portions of ether (three times), and the resulting brownish green microcrystalline solid was dried in vacuo to give 0.306 g (0.240 mmol, 90%) of pure **4f**. ^1H NMR ($CDCl_3$): δ 1.09 (t, CH_3, 3H), 1.80 (m, CH_2, 2H), 2.21 (s, NCH_3, 3H), 2.31 (m, CH_2, 2H), 2.96 (s, NCH_3, 3H), 4.81, 4.83 (d, =C*H*H, $^2J_{H-H}$ = 3.7 Hz, 1H), 5.18 (dquint, CH_2 (dppm), J_{H-H} = 15.2 Hz, $^2J_{P-H}$ = $^3J_{P-H}$ = 4.3 Hz, 2H), 5.36 (dquint, CH_2 (dppm), J_{H-H} = 15.2 Hz, $^2J_{P-H}$ = $^3J_{P-H}$ = 4.7 Hz, 2H), 7.37 (t, aryl H (dppm), $^3J_{H-H}$ = 7.4 Hz, 8H), 7.48 (m, aryl H (dppm), 12H), 7.59 (m, aryl H (dppm), 12H), 7.78 (m, aryl H (dppm), 8H). $^{13}C\{^1H\}$ NMR (CD_2Cl_2): δ 11.7 (CH_3 (Et), 25.2 (CH_2 (Et)), 40.4 (CH_2 (allenyl)), 40.6, 43.0 (CH_3N), 48.5 (vquint, CH_2 (dppm), N_{P-C} = 11.3 Hz), 79.85 (C=CH_2, allenyl), 100.0 (Et*C*=C, allenyl), 121.9 (quint, C2, J_{P-C} = 1.8 Hz), 128.3, 128.8 (quint, *m*-C_6H_5, N_{P-C} = 2.4 Hz), 130.5, 130.9 (*p*-C_6H_5), 133.0 (quint, *ipso*-C_6H_5, N_{P-C} = 10.8 Hz), 133.2, 133.6 (quint, *o*-C_6H_5, N_{P-C} = 3.0 Hz), 134.3 (quint, *ipso*-C_6H_5, N_{P-C} = 11.2 Hz), 153.7 (quint, C3, J_{P-C} = 1.1 Hz), 204.3 (C=*C*=C, allenyl), 207.0 (quint, C1, J_{P-C} = 13.7 Hz). ^{13}C (H coupled) NMR: δ 204.3 (vquint, $^3J_{CH}$ = 4.5 Hz), 78.9 (C=CH_2, allenyl, J_{C-H} = 167.6 Hz), 48.5 (tquint, J_{C-H} = 136.3 Hz), 43.0 (NCH_3, J_{C-H} = 141.5 Hz), 40.6 (NCH_3, J_{C-H} = 141.2 Hz), 25.2 (CH_2, t, br, J_{C-H} = 128.1 Hz), 11.7 (CH_3, tquart, J_{C-H} = 126.6 Hz, $^3J_{C-H}$ = 4.2 Hz). $^{31}P\{^1H\}$ NMR (CD_3CN): δ −8.0 (s, P (dppm)). IR (KBr; cm^{-1}): ν(CC) 1995 (s), 1920 (m), ν(C=N) 1572 (m). UV/vis (CH_3CN; λ_{max}, nm (log ϵ)): 211 (4.71), 227 (4.66), 266 (4.48), 391 (4.02), 460 (sh, 2.92), 623 (2.78). Anal. Calcd for $C_{61}H_{59}ClF_6NP_4RuSb$: C, 56.26; H, 4.57; N, 1.08. Found: C, 55.92; H, 4.51; N, 1.07.

***trans*-[ClRu(dppm)$_2$C≡CC(NMeC$_5$H$_8$)=CH$_2$]$^+$PF$_6^-$ (3g).** This compound was prepared from *cis*-$RuCl_2$(dppm)$_2$ (0.221 g, 0.23 mmol), $NaSbF_6$ (0.243 g, 0.94 mmol), and 1-methyl-1,2,5,6-tetrahydropyridine (110 μL) in *o*-dichlorobenzene as solvent. The suspension was stirred for 3 days under ambient conditions and then filtered. The solvent was then removed by vacuum distillation at 45 °C. The crude, oily product was repeatedly stirred with 10 mL portions of hexane and then dried to give crude **3g** as a turqoise, powdery residue. This was loaded on a silica gel column and eluted with CH_2Cl_2/CH_3CN (8:1) as a green band. After this band was dried under vacuum, 0.163 g (55.0%) was obtained as a green powder. ^1H NMR (CD_3CN): δ 1.83 (m, br, CH_2, 2H), 2.13 (s, NMe, 3H), 2.56 (oct, CH_2N, $^3J_{H-H}$ = $^4J_{H-H}$ = 6.2 Hz, 2H), 3.02 (dvquint, NC*H*, $^2J_{H-H}$ = 17.0 Hz, $^6J_{P-H}$ = 2.5 Hz, 1H), 3.33 (d mult br, NC*H*, $^2J_{H-H}$ = 17.0 Hz, 1H), 3.82 (d br, C=CH*H*, $^2J_{H-H}$ = 3.0 Hz, 1H), 4.73 (d, C=CH*H*, $^2J_{H-H}$ = 3.0 Hz, 1H), 4.87 (dvquint, CH_2 (dppm), J_{H-H} = 14.9 Hz, $^2J_{P-H}$ = $^4J_{P'-H}$ = 4.4 Hz, 2H), 5.09 (dvquint, CH_2 (dppm), J_{H-H} = 14.9 Hz, $^2J_{P-H}$ = $^4J_{P'-H}$ = 4.6 Hz), 5.33 (d mult, br, =C*H*, $^3J_{H-H}$ = 10.3 Hz, 1H), 5.70 (dhpt, =C*H*, $^3J_{H-H}$ = 10.3 Hz, $^3J_{H-H}$ = $^4J_{H-H}$ = 1.9 Hz, 1H), 7.19−7.30 (m, aryl H (dppm), 16H), 7.38 (m, aryl H (dppm), 8H), 7.46 (m, aryl H (dppm), 8H), 7.56 (m, aryl H (dppm), 8H). $^{13}C\{^1H\}$ NMR ($CDCl_3$): δ 22.6 (NCH_2CH_2), 49.7 (vquint, CH_2 (dppm), N_{P-C} = 11.1 Hz), 50.5 ($N(CH_3)$), 55.2 (C3), 57.1, 58.3 (NCH_2), 95.7 (vquint, J_{P-C} = 1.8 Hz, C2), 108.3 (C=CH_2), 119.9, 125.3 (=CH), 128.7, 128.7, 129.2, 129.3, (m, *m*-C_6H_5), 130.67, 130.76, 130.86, 130.94 (*p*-C_6H_5), 133.67, 133.70, 134.06, 134.23 (m, *o*-C_6H_5), 134.84, 135.02, 136.44, 136.65 (m, *ipso*-C_6H_5), 146.2 (vquint, C1, J_{P-C} = 14.2 Hz). $^{31}P\{^1H\}$ NMR ($CDCl_3$): δ −6.1 (AA′BB′ spin system; P (dppm)). IR (KBr; cm^{-1}): ν(C≡C) 2037 (m), ν(C=C) 1602 (m), 1585 (w), 1572 (w). UV/vis (CH_3CN; λ_{max}, nm (log ϵ)): 228 (4.80), 265 (4.56), 313 (4.00), 607 (2.74), 677 (2.55). Anal. Calcd for $C_{60}H_{57}ClF_6NP_4RuSb$: C, 55.93; H, 4.46; N, 1.09. Found: C, 54.94; H, 4.44; N, 1.15.

X-ray Crystallographic Analysis of 4b. Table 2 reports details of the structure analysis for **4b**. An orange-red crystal of **4b**, obtained by crystallization from a CH_2Cl_2/hexane mixture, was fixed with Nujol on top of a glass fiber and transferred to the cold stream of the low-temperature device of a Siemens P4 automated four-circle diffractometer. Cell constants were calculated from 52 well-centered reflections with 2θ angles ranging from 23.7 to 25°. Data were collected at 173 K using ω-scans. Two check reflections measured at regular intervals showed no loss of intensity at the end of data collection. An empirical absorption correction based on ψ-scans was applied (12 reflections, maximum and minimum transmission factors 0.892 and 0.612). The structure was solved by direct methods, which revealed the positions of most of the non-hydrogen atoms. The missing ones were located in subsequent difference Fourier syntheses. Most of them were refined with anisotropic thermal parameters. The atoms C4, C5, C6, and C7, which are statistically disordered about two positions (f = 0.57/0.43) were refined with isotropic thermal parameters— equivalent bond lengths and angles were restrained to be equal within an arbitrary standard deviation of 0.01 Å. Hydrogen atoms were added at calculated positions and assigned isotropic displacement parameters equal to 1.2 (CH, CH_2) or 1.5 times (CH_3) the U_{iso} value of their respective parent carbon atoms and treated with appropriate riding models during the refinement.

Acknowledgment. R.F.W. wishes to acknowledge financial support of this work by the Deutsche Forschungsgemeinschaft, the Fonds der Chemischen Industrie, and Johnson&Matthey for a generous loan of $RuCl_3$. Collaboration between R.F.W. and S.Z. was sponsored by VW-Stiftung within the project on "Intra- and Intermolecular Electron Transfer".

Supporting Information Available: Tables of atom coordinates, thermal parameters, and bond lengths and angles for **4b** and figures displaying the atomic displacement during the vibrations within the 2000−1500 cm^{-1} range. This material is available free of charge via the Internet at http://pubs.acs.org.

OM000925N